CHAPTER 3

RESULTS & DISCUSSION

This chapter describes the results obtained from two different techniques, X-ray crystallography and neutron scattering; details are presented and discussed.

3.1 X-Ray Crystallographic Study

The atomic numbering of CD is as commonly used in carbohydrates, e.g., C21 denotes carbon atom 2 (C2) of glucose residue 1 (see Figures 1.3 and 1.11 on pages 6 and 20, respectively). The methoxy C atoms are labeled as follows: O2–C7, O6–C8 for dimethyl-CDs and O2–C7, O3–C8, O6–C9 for trimethyl-CDs. The disordered atoms are labeled A and B.

3.1.1 Crystal Structures of DIMEB

3.1.1.1 DIMEB·2H_2O

Molecular Structure of DIMEB·2H_2O. The 7 glucose residues in DIMEB adopt the $^4C_1$ conformation with slight deviations from the theoretical chair form (see ring puckering parameters Q and Θ [32] in Table 3.1). The orientations of glucoses which are described by torsion angles ϕ and ψ [2] are in the normal range 101–113° and 120–136°, respectively, because the O3–H(n)$\cdots$O2(n + 1) hydrogen bonds between neighboring glucose residues (O$\cdots$O distances 2.79–3.02 Å; Table 3.1) stabilize and maintain the "round" geometry of DIMEB (Figure 3.1) as observed in the parent β-CD. The regular structure of the DIMEB macrocycle is indicated by the small variance in O4(n)$\cdots$O4(n – 1) distances (4.27–4.51 Å), in O4(n + 1)$\cdots$O4(n)$\cdots$O4(n – 1) angles (123.1–132.3°) and the very small deviation ($\leq$ 0.24 Å) of O4 atoms from

the common least-squares plane. Other interglucose interactions which contribute to the stabilization of the macrocyclic geometry are weak intramolecular, interglucose hydrogen bonds C6–H(n)···O5(n + 1). The contact distances C6(n)···O5(n + 1), H6(n)···O5(n + 1) and the angles at H6 atoms are in the range 3.31–3.52, 2.44–2.82 Å and 128–157°, respectively (Table 3.1). These data are in good agreement with those observed in unsubstituted CDs [156]. In addition, a number of C–H···O interactions also take part in the stabilization of the crystal structure, see Table A.5 on page 117.

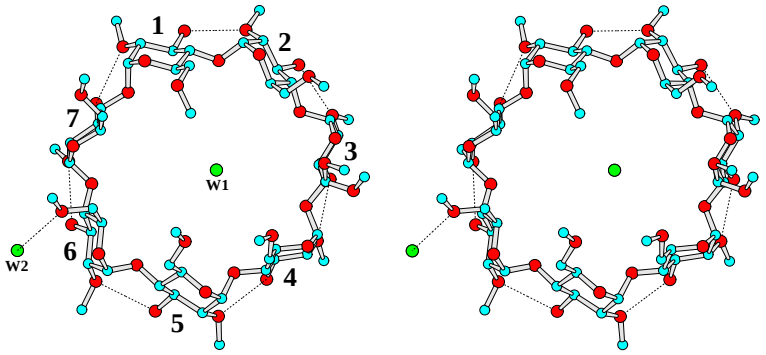

Figure 3.1: Stereo plot of DIMEB·2H_2O
Carbon, oxygen, and water oxygen atoms as cyan, red, and green spheres, respectively; the seven glucose residues are labeled with numbers 1–7, for numbering of glucose atoms see Figures 1.3 and 1.11. "Round" conformation of DIMEB is stabilized by O3(n)–H···O2(n + 1) hydrogen bonds (dashed lines) between adjacent glucose units.

All O2–C7 methoxy groups point "away" from the cavity with torsion angles C1–C2–O2–C7 at +*gauche* to *trans* (in range 84.7–154.9°). Three O5–C5–C6–O6 torsion angles belonging to glucose residues 1, 4 and 5 are in the +*gauche* range (65.6, 75.5 and 87.6°, respectively) and direct the O6–C8 groups toward the cavity, while the others are −*gauche*. O63–C83 is twofold disordered (occupancy factors 0.7 and 0.3 for sites A and B, respectively) giving rise to +*gauche* and −*gauche* conformations (see Figure 3.1). A similar disorder was also observed in anhydrous DIMEB [157]. The cavity of DIMEB is not closed by "inward" rotation of three O6–C8 groups as observed in anhydrous DIMEB [157].

While W1 is located within the macrocyclic cavity, W2 is found in a void between DIMEB molecules. The nearest interatomic distances between W1 and C5–H atoms

Table 3.1: Geometrical parameters of the DIMEB·2H_2O macrocycle

Distances in Å and angles in °. Definitions of puckering parameters: Q, Θ; torsion angles: ϕ, ψ; tilt angle; O4 angle, O4 deviation are explained in chapter 1 on pages 8–9.

Residue	1	2	3	4	5	6	7
Q	0.56	0.54	0.55	0.57	0.55	0.56	0.57
Θ	2	5	2	3	6	5	4
ϕ	112.5(4)	108.2(5)	107.2(5)	105.6(5)	112.9(5)	103.9(5)	101.4(4)
ψ	135.5(4)	123.8(5)	119.7(5)	132.0(4)	134.7(5)	123.1(5)	123.5(4)
Tilt angle	19.5(3)	16.6(3)	6.9(2)	10.3(3)	24.3(3)	16.4(2)	3.6(2)
O4 angle	127.7(1)	126.4(1)	128.6(1)	132.3(1)	123.1(1)	129.3(1)	130.9(1)
O4 deviation	–0.21(1)	0.00(1)	0.24(1)	–0.14(1)	–0.18(1)	0.24(1)	0.05(1)
Distances							
O4(n)···O4(n – 1)	4.37(1)	4.36(1)	4.35(1)	4.49(1)	4.42(1)	4.27(1)	4.51(1)
O3(n)···O2(n + 1)	2.79(1)	2.81(1)	2.90(1)	2.84(1)	3.02(1)	2.92(1)	2.94(1)
C6(n)···O5(n + 1)	3.46(1)	3.52(1)	3.33(1)	3.35(1)	3.46(1)	3.36(1)	3.31(1)
H6(n)···O5(n + 1)	2.61(1)	2.82(1)	2.51(1)	2.44(1)	2.55(1)	2.67(1)	2.59(1)
∠ C6–H(n)···O5(n + 1)	146.7(4)	129.9(4)	142.8(4)	155.9(6)	157.4(5)	128.1(4)	131.0(4)
Torsion angles							
C1–C2–O2–C7	138.7(8)	142.5(7)	154.9(7)	150.4(4)	125.8(6)	84.7(7)	150.8(5)
O5–C5–C6–O6	65.6(6)	–65.1(6)	46.5(11)[a]	75.5(9)	87.6(8)	–69.1(5)	–67.3(6)
			–58.3(11)[b]				
C5–C6–O6–C8	84.1(7)	–178.1(9)	–147.1(12)[a]	165.6(13)	179.3(11)	178.3(5)	–171.8(7)
			100.8(34)[b]				

[a,b] Values for disordered O6–C8 with occupancy factors 0.70 and 0.30 for sites A and B, respectively.

of glucose units 2, 3, 4 and C8–H of glucose unit 1 of the enclosing DIMEB are > 3.7 Å (Figure 3.2), too long to be of van der Waals or hydrogen bond type. The location of this polar water molecule in an apolar cavity is associated with a very high thermal motion, see ORTEP plot (Figure A.1) on page 108. W2 forms hydrogen bonds to O66 and O36, and reveals close contacts to endocyclic O5 oxygen atoms (O56, O54) of two adjacent DIMEB molecules, as well as weak interactions to C2–H and C7–H of glucose residue 4 (Figure 3.2).

Crystal Packing. The molecular arrangement in the crystal unit cell is shown in Figure 3.3. DIMEB dihydrate packs in "herring bone" fashion with molecules arranged along the 2_1 screw-axis parallel to the b-axis and slanted about 40° against the a-c plane. Both sides of each macrocycle cavity are blocked by glucose residues of neighboring molecules leading to a typical cage structure. No "self-inclusion" occurs as found in anhydrous DIMEB [157] or other complexes of DIMEB crystals [34, 64, 67,

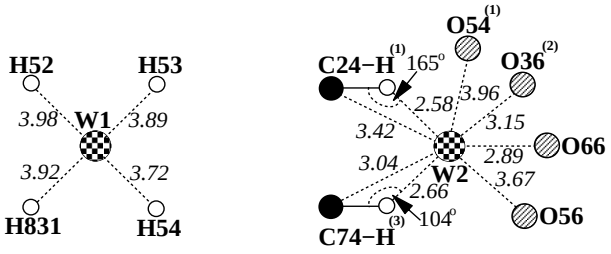

Figure 3.2: Environment of the two water molecules in DIMEB·2H_2O
W1 is included in the DIMEB cavity and shows high thermal motion (see Figure A.1, page 108) due to lack of hydrogen bonding to DIMEB (O···H distances > 3.7 Å). W2 is located in the intermolecular space and hydrogen bonded to the surrounding DIMEB. Atoms from symmetry related molecules are indicated with their symmetry operators: (1) $x + 1$, y, z; (2) $-x + 2$, $y - 0.5$, $-z + 2$; (3) $-x + 1$, $y - 0.5$, $-z + 2$. Given distances in Å and angles in °.

72]. This may be due to differences in space groups which are orthorhombic ($P2_12_12_1$) for anhydrous DIMEB [157] but monoclinic ($P2_1$) for DIMEB dihydrate; the latter displays the characteristic packing motif as in β-CD dodecahydrate [110, 112], DIMEA monohydrate [73, 155], and the complex between DIMEA and 1-propanol [65, 69].

DIMEB·2H_2O was crystallized from cold water (18°C). It includes one water molecule in the cavity and adopts an "open" cylinder-like form. There is no obvious stabilizing interaction between the included water molecule and the enclosing host cavity. Since the hydrogen bonding potential of this water is not satisfied, it probably escapes if the aqueous solution of DIMEB is heated up, followed by the collapse of DIMEB to a bowl-shaped conformation which is found in the anhydrous crystal form (obtained from aqueous solution at 60°C). Conversely, if any small, hydrophobic guest molecule is added to an aqueous solution of DIMEB, it easily displaces W1 from the cavity, forming an inclusion complex. In this respect, methylated CDs will be better-suited hosts for such guest molecules than their unsubstituted analogues [132].

Several attemps failed to reproduce the DIMEB·2H_2O crystals but the DIMEB·15 H_2O crystal (below) was obtained instead. This suggests that the DIMEB·2H_2O crystal form is energetically instable and may be only an intermediate state in crystallizing DIMEB from cold water.

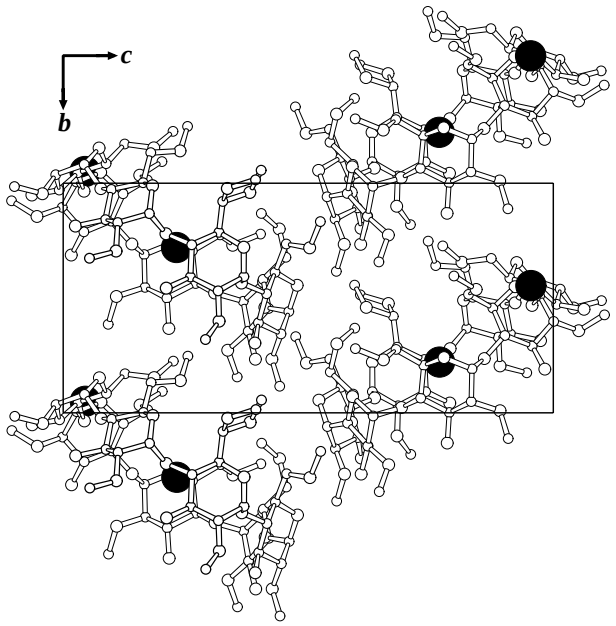

Figure 3.3: Crystal packing in "herring bone" style of DIMEB·2H_2O
DIMEB molecules are arranged along twofold screw-axis parallel to *b*-axis with their O4 mean planes inclined about 40° to *a*-*c* plane. Both ends of the DIMEB cavity are blocked by adjacent molecules forming isolated cages in which W1 is included. Small, large, unfilled, and largest filled spheres represent DIMEB carbon, oxygen, and water oxygen atoms, respectively.

3.1.1.2 DIMEB·15H_2O

Molecular Structure of DIMEB·15H_2O. All 7 glucose units of the DIMEB molecule are in the regular $^4C_1$ chair conformation as indicated by the Cremer-Pople puckering parameters Q and Θ [32] in the ranges 0.54–0.57 Å and 3–8°, respectively (Figure 3.4 and Table 3.2). They are in *syn* orientation, stabilized by systematic intramolecular, interglucose O3(n)–H···O2($n+1$) hydrogen bonds (O···O distances 2.81–3.04 Å) between adjacent glucose units in the macrocycle, giving rise to normal torsion angles ϕ and ψ [2] about the interglucose α-(1→4) linkage (97.2–110.6° and 115.1–136.3°), Figure 3.4 and Table 3.2. The DIMEB macrocycle is "round" as indicated by narrow variance of O4(n)···O4($n-1$) distances (4.30–4.47 Å) showing the well-defined O4 heptagon, by slight deviations of glycosidic O4 from their common least-squares plane (–0.19 to 0.13 Å), and by short span of tilts angles (2.6–27.5°), Figure 3.4 and Table 3.2. Another contribution to the conformational stability of

the macrocycle are the systematic intramolecular, interglucose C6–H(n)···O5(n + 1) hydrogen bonds as shown by C6(n)···O5(n + 1), H6(n)···O5(n + 1) distances and C6-H(n)···O5(n + 1) angles in the ranges 3.30–3.57, 2.47–2.76 Å and 128.6–151.8°, respectively (Table 3.2). In addition, a number of intermolecular O–H···O and C–H···O hydrogen bonds (Table A.6 on page 117) also contribute to stabilization of the crystal structure.

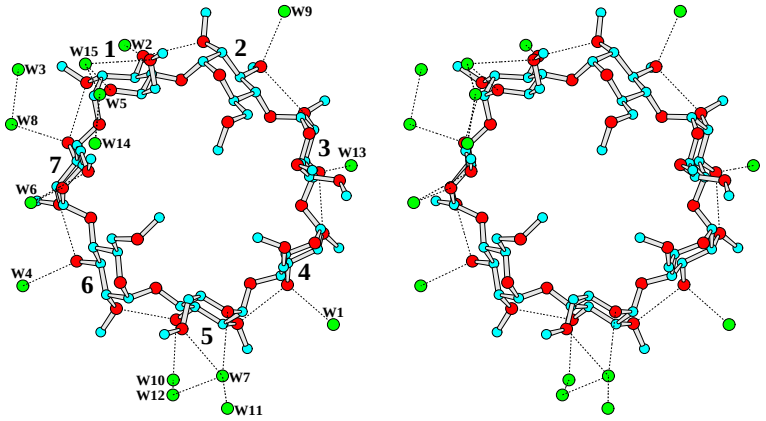

Figure 3.4: Stereo plot of DIMEB·15H_2O

Carbon, oxygen, and water oxygen atoms as cyan, red, and green spheres, respectively; the seven glucose residues are labeled with numbers 1–7, for numbering of glucose atoms see Figure 3.5(a). Dotted lines indicate O–H···O hydrogen bonds within 3.5 Å distance. "Round" macrocyclic conformation is stabilized by intramolecular, interglucose O3–H(n)···O2(n + 1) hydrogen bonds. O3–H groups of glucose units 1–7 are systematically hydrogen bonded to water molecules W2, W9, W13, W1, W10, W4, W8 (see also Figure 3.5(a)).

All O2–CH_3 groups point "away" from the cavity with torsion angles C1–C2–O2–C7 in the +*gauche* to *trans* range (96.7–141.8°). The O6–CH_3 groups of glucose residues 2, 4, and 6 are rotated "inward" the cavity with torsion angles O5–C5–C6–O6 in +*gauche* (61.9–72.6°) – that of residue 3 is twofold disordered with half occupancies; they are in +*gauche* and –*gauche* for sites A and B, respectively. At the O6-side, the DIMEB cavity is closed by "inward" rotation of three O6–CH_3 groups of glucose residues 2, 4 and 6 (Figure 3.4); this strongly reduces the cavity volume. The remaining volume is occupied at O2-, O3-side by a doubly disordered O63–CH_3 group of an adjacent DIMEB related by twofold screw axis ("self-inclusion"), see Figure 3.6.

Table 3.2: Geometrical parameters of the DIMEB·15H_2O macrocycle

Distances in Å and angles in °. Definitions of puckering parameters: Q, Θ; torsion angles: ϕ, ψ; tilt angle; O4 angle, O4 deviation are explained in chapter 1 on pages 8–9.

Residue	1	2	3	4	5	6	7
Q	0.55	0.57	0.57	0.54	0.56	0.57	0.55
Θ	3	8	3	4	5	5	3
ϕ	109.7(6)	108.4(6)	97.2(7)	105.7(6)	109.0(6)	110.6(6)	101.5(6)
ψ	136.3(5)	135.9(6)	119.1(6)	128.3(6)	126.9(6)	130.6(6)	115.1(6)
Tilt angle	18.0(2)	27.5(3)	11.0(4)	11.0(3)	14.0(2)	18.4(2)	2.6(3)
O4 angle	128.3(1)	131.7(1)	127.6(1)	125.9(1)	129.3(1)	132.5(1)	123.8(1)
O4 deviation	–0.19(1)	0.06(1)	0.11(1)	–0.06(1)	–0.12(1)	0.13(1)	0.07(1)
Distances							
O4(n)···O4(n – 1)	4.30(1)	4.47(1)	4.41(1)	4.36(1)	4.37(1)	4.44(1)	4.40(1)
O3(n)···O2(n + 1)	2.87(1)	3.04(1)	2.85(1)	2.95(1)	2.83(1)	2.81(1)	2.95(1)
C6(n)···O5(n + 1)	3.30(1)	3.37(1)	3.35(1)	3.43(1)	3.38(1)	3.57(1)	3.33(1)
H6(n)···O5(n + 1)	2.51(1)	2.67(1)	2.54(1)	2.55(1)	2.59(1)	2.76(1)	2.47(1)
∠ C6–H(n)···O5(n + 1)	138.7(5)	128.6(5)	141.4(5)	151.8(6)	139.2(5)	141.0(6)	146.4(5)
Torsion angles							
C1–C2–O2–C7	96.7(9)	113.5(17)	122.0(12)	141.8(7)	105.8(10)	113.2(9)	136.4(6)
O5–C5–C6–O6	–63.5(7)	61.9(10)	58.2(10)[a]	67.7(8)	–64.1(11)	72.6(7)	61.7(11)
			–71.9(8)[b]				
C5–C6–O6–C8	–179.6(8)	87.9(13)	–158.8(20)[a]	90.1(14)	–166.1(10)	79.7(22)	171.5(8)
			–174.8(12)[b]				

[a,b] Values for disordered O6–C8 with occupancy factors 0.50 for both sites A and B.

Unique Clathrate Hydrate of DIMEB·15H_2O. The hydration of DIMEB stacks by the 15 H_2O is remarkable. The O3-H groups of DIMEB form systematic hydrogen bonds to 7 water molecules with O···O distances 2.81–2.89 Å, Figures 3.4 and 3.5(a). Together with additional 8 water molecules, a hydrogen-bonded, regular water network is constructed that encapsulates the DIMEB molecules in the form categorized as clathrate hydrate channel structure [92]. The network is formed by a repeating motif described as $4^1 6^2 8^1$ (see caption Figure 3.5) which by the operation of the twofold screw-axes (see caption Figure 3.6) yields corrugated sheets parallel to the *a*-*c* plane; they are linked by water chains W1–W2–W4 into channels harboring the stacks formed by DIMEB molecules.

The clathrate hydrate channel structure of DIMEB·15H_2O is highly specific as no other methylated CD has the same constellation of O3–H groups that is required to anchor and stabilize the water network. It is unique in four respects: (i) there are no water pentagons that usually dominate clathrate and semiclathrate structures [92];

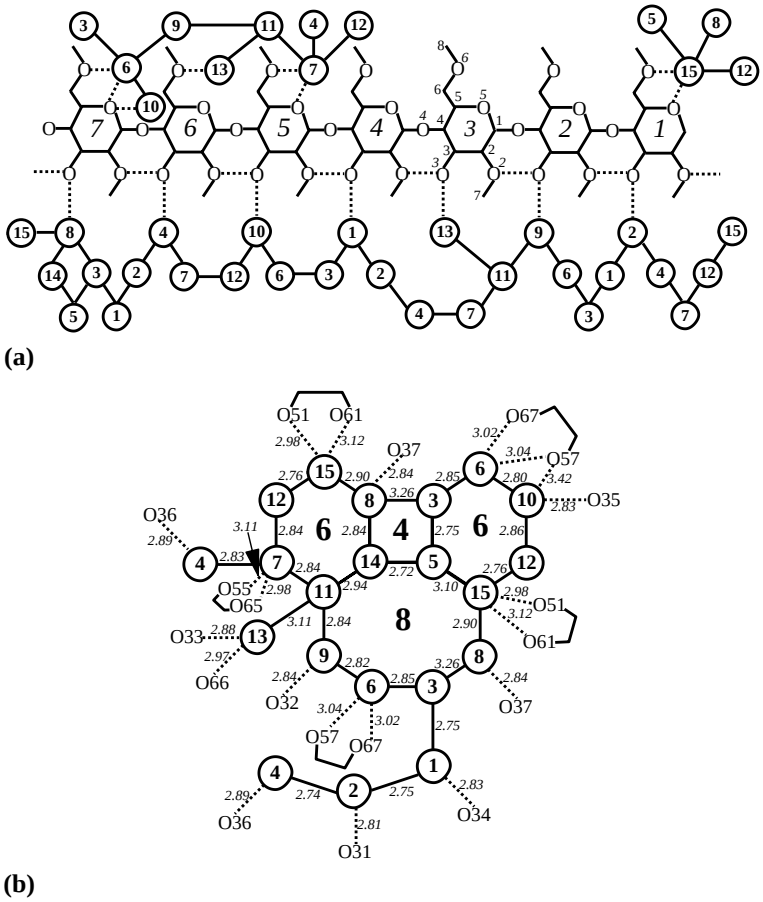

Figure 3.5: Schematic presentation of hydrogen bonds in DIMEB·15H_2O (a) The hydration of DIMEB, glucose units are numbered sequentially *1–7*, atomic numbering is given for glucose unit 3; methyl C-atoms attached to O2 and O6 are assigned as C7 and C8, respectively. Strong hydrogen bond donors/acceptors O3–H are systematically hydrated, the weak O5, O6 acceptors only partially (glucose units 1, 5, 6, 7), and O2, O4 never. (b) The water network showing edge-sharing polygons with one tetra-, two hexa-, one octagons ($4^1 6^2 8^1$) described by bold numbers **4**, **6**, **8**; water molecules are denoted as circled numbers; dashed and solid lines indicate hydrogen bonds $O_w \cdots O_{DIMEB}$ and $O_w \cdots O_w$, respectively. The chain of W1–W2–W4 and the individual W13 are not involved in formation of these polygons. Given distances in Å.

(ii) in contrast to all other clathrate hydrates where either no or only few hydrogen bonds are formed between guest and clathrate water molecules, DIMEB·15H_2O abounds with such interactions (see Figure 3.5 and the broken pink sticks in Figure 3.6). Of the 15 H_2O, only 5 are *not* hydrogen bonded to DIMEB, the other 10 being in contact with the seven O3–H groups and with O5, O6 atoms, see Figures 3.4,

3.5; (iii) a total of 15 hydrogen bonds anchors DIMEB tightly and specifically to the clathrate hydrate network and gives rise to high thermal stability: upon heating, a crystal-to-crystal phase transition occurs at 110°C with changes of unit cell constants b and c by –17.0% and +30.7%, respectively, and the unit cell volume increases by 8.5%, indicating structural changes; at 280°C, X-ray diffraction breaks down because crystals decompose – by contrast, the most stable known clathrates (of the alkylammonium type) melt in the range –20 to 30°C [92]; (iv) DIMEB is the largest guest found thus far hosted by a clathrate hydrate.

3.1.1.3 Structural Comparison of Uncomplexed DIMEB

Three crystal structures of uncomplexed DIMEB have been reported so far, DIMEB anhydrate [157], DIMEB·2H_2O [11, 12], and DIMEB·15H_2O [9]. The former one crystallized from hot water at 60°C while the latter two crystallized from cold water at 18°C. The rms deviations of superposition of the three DIMEB molecules (all O6 and methyl C atoms are excluded from the calculation) are in the range of 0.20–0.40 Å, showing that they are very similar, Figure 3.7. However, three striking differences are observed: (i) DIMEB anhydrate and DIMEB·15H_2O resemble a "bowl" while DIMEB·2H_2O is an "open" cylinder; this is due to closing of the molecular cavity at O6-side by "inward" rotation of three O6–CH_3 groups found in the former two but not in the latter. (ii) The "self-inclusion" complexes are observed in both DIMEB anhydrate and DIMEB·15H_2O; their cavities are occupied by a doubly disordered O6-CH_3 group of a neighboring DIMEB molecule. By contrast, in DIMEB·2H_2O, one water molecule is included in the cavity, forming an inclusion complex. (iii) The packing of DIMEB·2H_2O is similar to "herring-bone" mode (cage type) – a typical crystal packing usually observed in native CDs [136]. By contrast, those of DIMEB anhydrate and DIMEB·15H_2O are unique and can be classified neither as channel nor cage type because DIMEB molecules are stacked in columns along a twofold screw axis and their O4 planes are inclined against the b-c planes (Figure 3.6(a)) so that these stacks do not resemble a roll of coins as found in channel type of native CDs [136].

The similarity in molecular structures of DIMEB anhydrate and DIMEB·15H_2O suggests that no matter whether DIMEB crystallizes from hot or cold water, it should have the same molecular conformation but more interesting is the presence of the molecular hydration which is only present if DIMEB crystallizes from cold water as

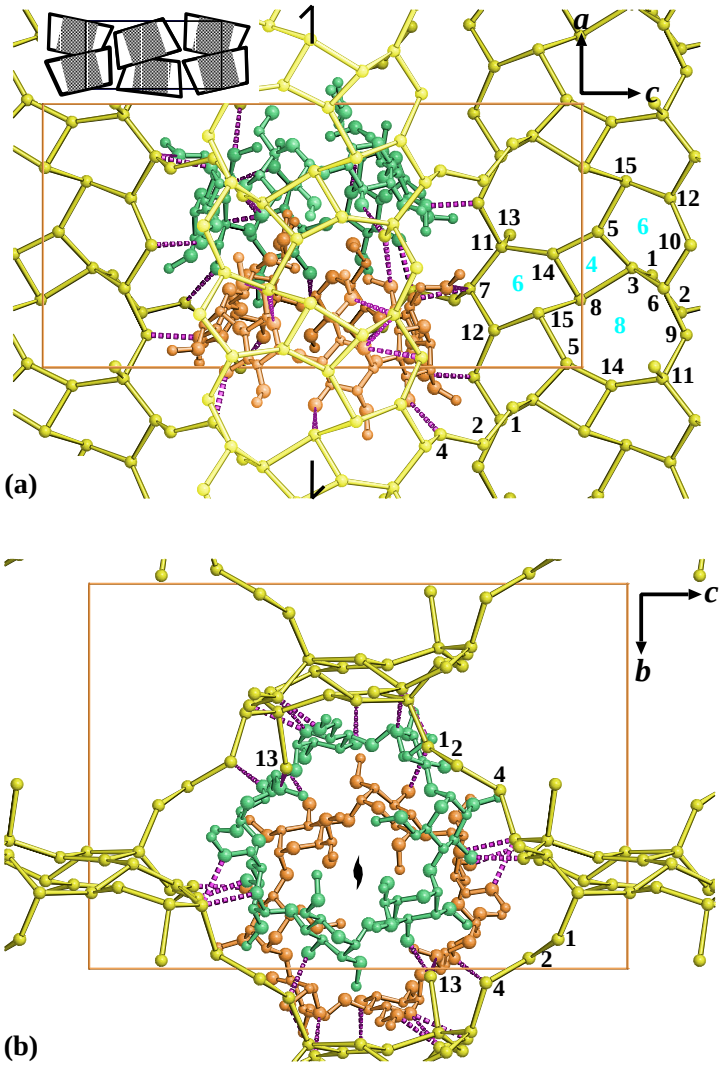

Figure 3.6: Clathrate hydrate channel structure of DIMEB·15H_2O
Views on (a) *a*-*c* and (b) *b*-*c* planes. Two DIMEB molecules related by the twofold screw operation parallel to the *a*-axis are shown in green and orange ball-and-stick representation; larger balls are oxygen and smaller, carbon atoms. Water molecules (labeled with black numbers) and inter-water hydrogen bonds are shown as yellow balls and sticks, respectively. Broken pink sticks indicate hydrogen bonds between oxygen atoms of DIMEB and water molecules. The repeating unit ($4^1 6^2 8^1$) of the water network is indicated by cyan numbers ($O_w \cdots O_w$ distances 2.75–3.26 Å). This motif is extended by 2_1 operation parallel to *a* forming a "ribbon" in the *a*-*c* plane (ribbons closer to the viewer (bright yellow) and further away (dark yellow), (b). Each "ribbon" is connected by water chains W1–W2–W4 to other ribbons symmetry related by the operation of twofold screw axes parallel to *c*, giving rise to clathrate hydrate channels which accommodate the stacks of DIMEB, see (b). The inset in (a) shows a schematic presentation of crystal packing (water molecules omitted).

DIMEB·15H_2O. Such a massively hydrated crystal structure may explain why methylated CDs are so soluble in cold water. By contrast, the crystals grown from hot water have no or only few water of hydration molecules [25, 73, 155, 157, 158, 160]; this correlates with the poor solubility of methylated CDs at these conditions. Another evidence for the presence of the molecular hydration in methylated CD crystals obtained from cold water is the two crystal forms of TRIMEG, (4TRIMEG)·19.3H_2O and TRIMEG·4.5H_2O; their structural descriptions are discussed below.

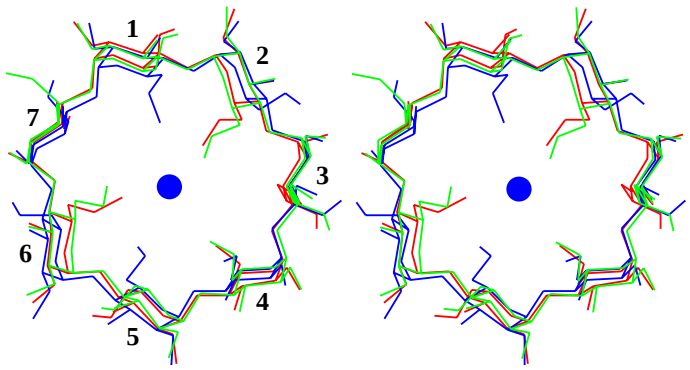

Figure 3.7: Stero plot of the overlay of uncomplexed DIMEB
Similar macrocyclic conformations of uncomplexed DIMEB with rms deviations of superposition 0.20-0.40 Å: DIMEB anhydrate [157] (red), DIMEB·2H_2O [11, 12] (blue), and DIMEB·15H_2O [9] (green). A water molecule in the central cavity of DIMEB·2H_2O is shown as filled circle.

3.1.2 Crystal Structures of TRIMEG

3.1.2.2 (4TRIMEG)·19.3H_2O

The atomic numbering in this structure is the same as described before, but a number is added to distinguish the four TRIMEG molecules in the asymmetric unit, i.e., first the chemical number, second the number of the glucose unit (1–8), and third the TRIMEG molecule (1, 2, 3, 4), Figures 3.8(a)–(d). For example, O37_4 denotes atom O3 in glucose residue 7 of TRIMEG 4.

Molecular Structure of (4TRIMEG)·19.3H_2O.

• **The Conformations of the Four TRIMEG Molecules are Almost Identical with Pseudo-Twofold Rotation Symmetries.** All four TRIMEG molecules

in the asymmetric unit are similar in shape and can be superimposed with rms deviations in the range 0.34–0.52 Å (omitting O6 and all CH_3 groups), Figure 3.9(a). The TRIMEG molecules have an "elliptical" rather than the "round" shape known for the native CDs. The long axis of the ellipse passes through glucose units 3 and 7 and the short axis through units 1 and 5 (see also Fig 3.8(a)–(d)). The molecules have local pseudo-twofold rotation axes passing through water molecules located within the molecular cavities. The water molecules are hydrogen bonded to O61 and O65 which belong to C5–C6–O6–C9 chains rotated "inward" to close the molecular cavities from one side so that the TRIMEG molecules adopt the bowl-shape characteristic of methylated CDs crystallized from hot water [25, 73, 155, 157, 158, 160], see Figures 1.15–1.19 (pages 26–28).

Glucose units 2–4 and 6–8 are in *syn* orientation, i.e., their O2–CH_3, O3–CH_3 groups are on one side of the macrocycle and O6–CH_3 on the other. By contrast, glucose units 1 and 5 are flipped by $\approx 180°$ into an *anti* orientation so that atoms O61 and O65, which are rotated toward the cavity, can accept hydrogen bonds from the water molecule located on the pseudo-twofold rotation axis. Individual geometrical data are given in Tables 3.3(a)–(j). All glucose residues adopt the $^4C_1$-chair conformation, with some slight distortions as indicated by their puckering parameters [32] Q within 0.49–0.58 Å and Θ within 2–17°. The deviations of individual O4 atoms from their mean plane are ≤ 1.34 Å, the tilt angles of glucoses with respect to this plane are in the range 12.9–57.2°, O4(n)$\cdots$O4($n-1$) distances are within 4.04–4.55 Å; O4($n+1$)$\cdots$O4(n)$\cdots$O4($n-1$) angles are in the range 119.1–145.5°. The largest variations are found with torsion angles ϕ, ψ describing the orientation of adjacent glucose units with respect to their glycosidic linkage (defined as ϕ, O5(n)–C1(n)–O4($n-1$)–C4($n-1$) and ψ, C1(n)–O4($n-1$)–C4($n-1$)–C3($n-1$) [2]), Table 3.3(f). They are in the range commonly observed for *syn*-oriented glucoses ϕ, 51.2–99.5°; ψ, 69.8–122.4° and differ for the two *anti*-oriented glucose units 1 and 5 ϕ, 81.4–95.8°; ψ, –59.5 to –71.9°.

Table 3.3: Geometrical parameters of the (4TRIMEG)·19.3H_2O macrocycles, distances in Å and angles in °; values for disordered O–CH_3 groups are marked with superscripts *a*–*g*. Definitions of puckering parameters: Q, Θ; torsion angles: ϕ, ψ; tilt angle are explained in chapter 1 on page 8.

Residue	TRIMEG 1	TRIMEG 2	TRIMEG 3	TRIMEG 4
	(a) Glucoses puckering parameters, Q and Θ			
1	0.51, 5	0.54, 2	0.56, 7	0.58, 6
2	0.52, 14	0.53, 11	0.55, 10	0.53, 13
3	0.53, 11	0.52, 10	0.54, 9	0.52, 11
4	0.55, 4	0.55, 8	0.54, 10	0.54, 14
5	0.57, 4	0.57, 4	0.56, 6	0.57, 6
6	0.51, 14	0.51, 10	0.54, 4	0.56, 3
7	0.54, 10	0.49, 16	0.53, 17	0.52, 17
8	0.52, 12	0.54, 13	0.52, 12	0.53, 10
	(b) Tilt angles			
1	37.8(2)	26.0(2)	41.6(4)	34.2(5)
2	52.2(2)	57.2(2)	40.3(2)	56.1(2)
3	18.7(4)	20.1(4)	12.9(2)	18.2(2)
4	45.6(3)	38.8(3)	33.6(2)	35.1(2)
5	46.7(3)	31.9(3)	33.2(3)	35.0(3)
6	48.9(3)	56.8(3)	48.0(5)	42.5(6)
7	16.4(4)	15.8(4)	17.8(3)	18.9(3)
8	46.6(2)	37.2(2)	44.9(4)	41.5(5)
	(c) O4(n)···O4(n – 1) distances between adjacent glucose residues			
1	4.32(1)	4.35(1)	4.17(1)	4.40(1)
2	4.04(1)	4.13(1)	4.19(1)	4.16(1)
3	4.22(1)	4.19(1)	4.24(1)	4.18(1)
4	4.55(1)	4.38(1)	4.40(1)	4.37(1)
5	4.50(1)	4.43(1)	4.53(1)	4.47(1)
6	4.16(1)	4.30(1)	4.40(1)	4.40(1)
7	4.26(1)	4.15(1)	4.04(1)	4.10(1)
8	4.40(1)	4.29(1)	4.31(1)	4.24(1)
	(d) Deviation of O4 atoms from their least-squares plane			
1	–1.08(1)	–1.09(1)	0.85(1)	0.99(1)
2	0.07(1)	0.13(1)	–0.10(1)	–0.06(1)
3	1.24(1)	1.34(1)	–1.01(1)	–1.11(1)
4	–0.29(1)	–0.43(1)	0.36(1)	0.39(1)
5	–0.94(1)	–0.96(1)	0.65(1)	0.63(1)
6	0.04(1)	0.13(1)	0.02(1)	0.07(1)
7	1.18(1)	1.21(1)	–1.06(1)	–0.96(1)
8	–0.22(1)	–0.32(1)	0.29(1)	0.05(1)

Table 3.3: (continue)

Residue	TRIMEG 1	TRIMEG 2	TRIMEG 3	TRIMEG 4
		(e) O4(n + 1)···O4(n)···O4(n – 1) angles		
1	135.4(2)	138.7(2)	142.0(2)	135.7(2)
2	119.5(2)	124.8(2)	121.8(2)	127.6(2)
3	131.6(2)	120.1(2)	127.1(2)	122.3(2)
4	131.0(2)	133.2(2)	133.4(2)	133.0(2)
5	138.0(2)	140.2(2)	142.0(2)	145.5(2)
6	119.8(2)	126.5(2)	122.2(2)	121.1(2)
7	130.1(2)	119.1(2)	125.1(2)	126.5(2)
8	137.6(2)	139.2(2)	139.7(2)	141.1(2)
		(f) Torsion angles, ϕ and ψ		
1	87.3(7), –64.3(8)	92.1(8), –60.4(9)	88.2(9), –64.9(11)	95.8(9), –59.5(12)
2	55.7(9), 74.6(9)	53.6(10), 71.7(10)	57.4(10), 69.8(10)	53.3(9), 79.8(10)
3	90.5(7), 110.1(7)	88.0(8), 103.4(8)	96.6(8), 122.4(8)	86.9(7), 99.4(7)
4	92.9(7), 109.1(7)	94.9(8), 120.6(7)	93.2(7), 112.1(7)	99.5(7), 115.7(7)
5	81.4(8), –71.9(9)	85.6(9), –65.8(10)	87.7(8), –65.6(9)	86.3(8), –67.4(9)
6	59.4(9), 79.8(9)	51.4(11), 80.0(10)	48.0(11), 74.5(10)	51.2(12), 70.2(12)
7	92.5(8), 114.5(8)	87.6(9), 106.5(8)	95.3(9), 117.9(9)	97.6(10), 121.7(10)
8	92.9(8), 103.3(7)	97.0(8), 109.9(8)	91.5(9), 99.2(9)	94.4(9), 93.5(10)
		(g) Torsion angles C1–C2–O2–C7		
1	93.9(13)	103.1(14)	88.9(16)	118.5(16)
2	104.0(14)	85.4(12)	97.7(15)	76.4(10)
3	84.9(12)	107.2(13)	76.1(12)	116.4(13)
4	83.2(11)	74.8(10)	75.1(10)	75.5(9)
5	110.6(13)	114.3(19)	118.8(13)	118.7(15)
6	101.5(15)	110.4(15)	120.4(19)	–65.3(26)[a], –60.3(28)[a]
7	91.9(13)	94.6(14)	79.9(12)	78.9(13)
8	98.8(10)	84.4(11)	90.5(11)	102.4(11)
		(h) Torsion angles C2–C3–O3–C8		
1	–101.2(11)	–100.4(15)	59.5(15)	–97.4(12)
2	–90.6(10)	–94.4(10)	–103.5(14)	–98.5(9)
3	–89.8(10)	–102.4(9)	–95.1(10)	–96.8(9)
4	–74.3(14)	–87.1(10)	–85.4(10)	–85.0(10)
5	–107.6(14)	–102.6(14)	–101.8(13)	–100.0(13)
6	–99.2(11)	–98.2(12)	–108.5(15)	–113.1(17)
7	–92.5(12)	–89.1(13)	–90.5(11)	–93.3(12)
8	–83.6(10)	–85.0(10)	–81.3(12)	–91.5(12)
		(i) Torsion angles O5–C5–C6–O6		
1	–62.6(8)	–64.1(9)	–68.2(11)	–61.2(10)

Table 3.3: (continue)

Residue	TRIMEG 1	TRIMEG 2	TRIMEG 3	TRIMEG 4
2	83.4(10)	78.9(12)	–69.3(11)	66.6(13)
3	71.6(10)	–59.1(17)[b], 69.5(15)[b]	73.9(10)	67.6(10)
4	–76.9(10)	–66.3(14)[c], 78.2(21)[c]	–69.3(10)	–73.5(10)
5	–64.9(9)	–66.4(10)	–66.3(9)	–68.3(10)
6	75.8(11)	95.8(13)	65.0(13)	67.7(15)
7	–61.1(9)	67.7(15)	78.8(11)	77.7(16)
8	71.0(11)	67.4(12)	70.3(14)	–38.1(22)[d], –72.7(17)[d]
		(j) Torsion angles C5–C6–O6–C9		
1	169.8(8)	172.6(9)	176.4(9)	174.4(9)
2	–70.9(22)	–175.6(29)	–175.2(13)	112.9(24)
3	–117.2(17)	165.2(35)[e], –172.6(32)[e]	84.1(12)	–89.5(11)
4	106.5(17)	–172.3(18)[f], 171.9(45)[f]	92.7(12)	86.4(12)
5	174.2(8)	179.3(9)	178.5(8)	176.9(9)
6	–83.4(17)	–81.2(24)	111.6(22)	103.2(27)[g], –144.5(20)[g]
7	179.7(10)	157.3(19)	–171.6(14)	–169.3(19)
8	–177.4(12)	177.9(16)	–150.6(20)	–143.6(21)[h], 173.8(16)[h]

[a] Disordered C76_4 with occupancy factors 0.45 and 0.55 for sites A and B, respectively.
[b] Disordered O63_2 with occupancy factors 0.45 and 0.55 for sites A and B, respectively.
[c] Disordered O64_2 with occupancy factors 0.75 and 0.25 for sites A and B, respectively.
[d] Disordered O68_4 with occupancy factors 0.50 for both sites A and B.
[e] Disordered O63–C93_2 with occupancy factors 0.45 and 0.55 for sites A and B, respectively.
[f] Disordered O64–C94_2 with occupancy factors 0.75 and 0.25 for sites A and B, respectively.
[g] Disordered C96_4 with occupancy factors 0.53 and 0.47 for sites A and B, respectively.
[h] Disordered O68_4 with occupancy factors 0.50 for both sites A and B.

• **The Orientation of the Methyl Groups at O2 and O3 is Restricted.** The orientation of the methyl groups relative to the associated glucose is best described for the secondary O2–CH_3, O3–CH_3 by torsion angles C1–C2–O2–C7 and C2–C3–O3–C8 and for the primary O6–CH_3 by the two torsion angles O5–C5–C6–O6 and C5–C6–O6–C9. Torsion angles C1–C2–O2–C7 are in the +*gauche* range, 74.8–120.4° except for glucose residue 6 of TRIMEG 4 where C7 is twofold disordered and the torsion angle is –*gauche* (–65.3°; –60.3°). This means (except for glucose

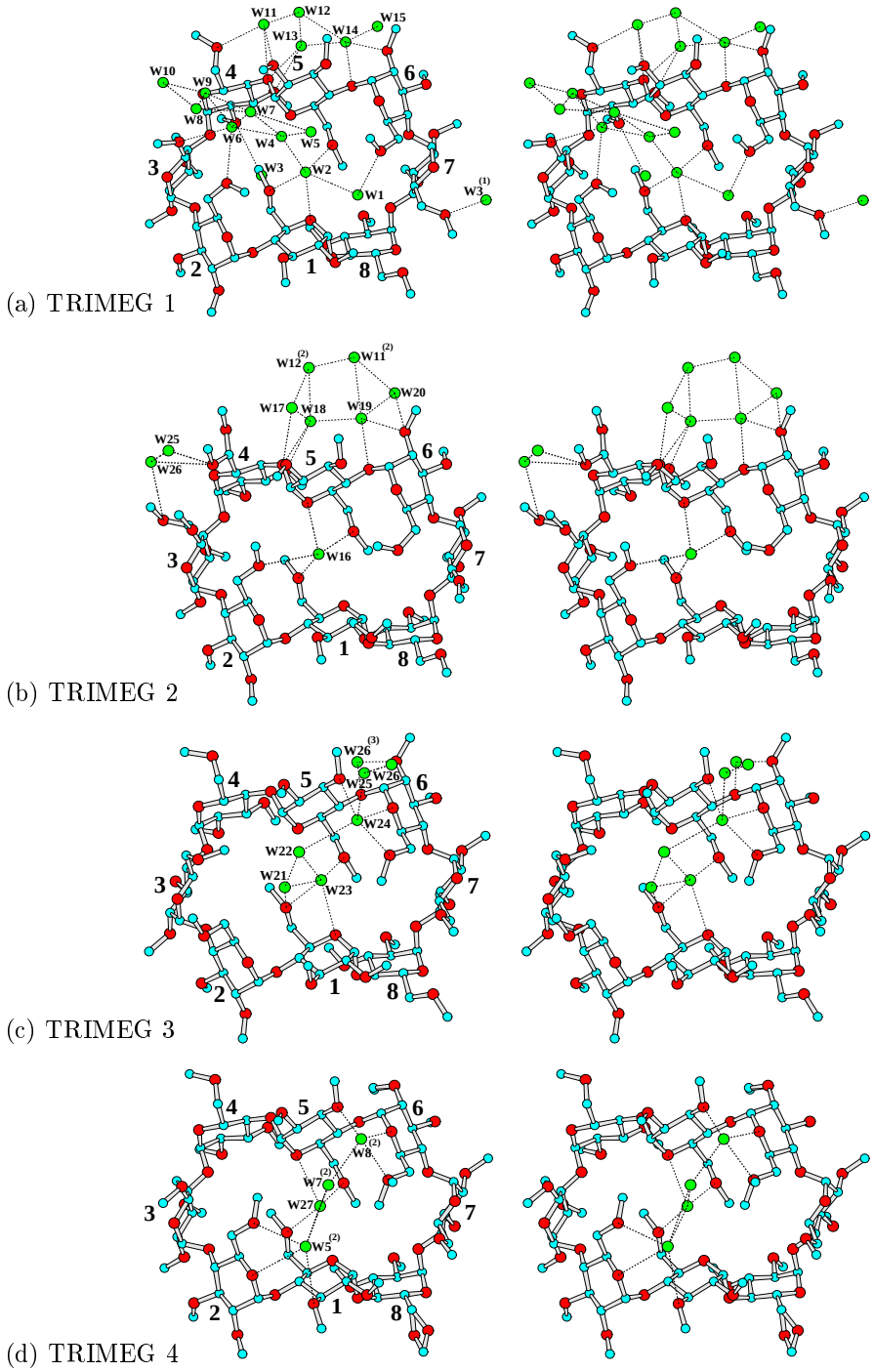

(a) TRIMEG 1

(b) TRIMEG 2

(c) TRIMEG 3

(d) TRIMEG 4

Figure 3.8: Stereo plots of individual TRIMEG in (4TRIMEG)·19.3H_2O (a) TRIMEG 1, (b) TRIMEG 2, (c) TRIMEG 3, and (d) TRIMEG 4. The cyan, red, and green spheres are C, O, and O_w, respectively. The dashed lines indicate possible hydrogen bonds within 3.5 Å distance. Water sites with superscripts (1), (2), and (3) are in symmetry equivalent positions : $-x$, $0.5 + y$, $1 - z$; $1 + x$, y, z; and $1 - x$, $-0.5 + y$, $1 - z$; respectively (see also Figures 3.10(a)–(c) for structural details of hydrogen bond networks of water sites).

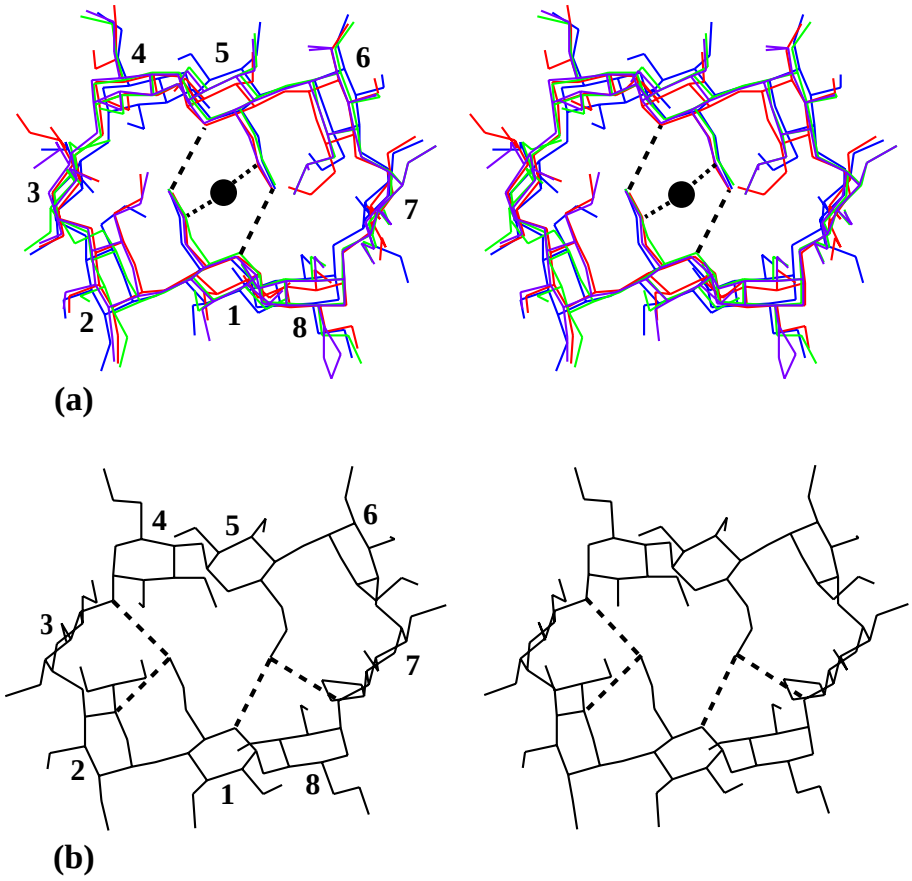

Figure 3.9: Stero plots of (4TRIMEG)·19.3H_2O and TRIMEG·2H_2O
(a) Overlay of four TRIMEG molecules in (4TRIMEG)·19.3H_2O [13]; blue, red, green and violet lines represent TRIMEG 1, TRIMEG 2, TRIMEG 3 and TRIMEG 4, respectively. The filled circle indicates the common water molecule located on the pseudo-twofold rotation axes of TRIMEG molecules. Dotted and dashed lines show systematic hydrogen bonds of O_w–H···O61, O_w–H···O65, and C91–H···O55, C95–H···O51, respectively. (b) TRIMEG molecular structure in TRIMEG·2H_2O [160]; two water molecules located outside the cavity not shown, dashled lines indicate C–H···O hydrogen bonds.

residue 6 of TRIMEG 4) that C7 is on the same side of the plane described by glucose atoms C2, C3, C5, and O5 as atom C6 (*endo*). By contrast, torsion angles C2–C3–O3–C8 are *–gauche* (–74.3 to –113.1°) so that C8 is on the opposite side of this plane (*exo*), except for glucose unit 1 of TRIMEG 3 where this torsion angle is *+gauche* (59.5°). Torsion angles describing the orientations of O6 and C9 are more variable (Tables 3.3(i) and (j)) except for glucose units 1 and 5 which are oriented *anti*. For these glucoses, O5–C5–C6–O6 is *–gauche* (–61.2 to –68.3°) and C5–C6–O6–

C9 is *trans* (169.8–179.3°) and so narrowly confined that the O61 and O65 atoms are in the correct position to form hydrogen bonds to the water molecules located on the pseudo-twofold axes (Figures 3.8(a)–(d) and 3.9(a)). The corresponding torsion angles of the other glucoses are much more variable, in *+gauche* and *−gauche* for O5–C5–C6–O6 and, in addition, *trans* for C5–C6–O6–C9.

• **Stabilization of Macromolecular Conformation by Hydrogen Bonds.** The conformation and pseudo-twofold symmetry of the four TRIMEG molecules is stabilized by the *anti* orientation of the diametrically opposed glucose units 1 and 5 (Figures 3.8(a)–(d) and 3.9(a)). Their O6 atoms, O61 and O65, accept hydrogen bonds (in the O···O distance range 2.738–3.178 Å) from the water molecules located on the respective pseudo-twofold axes, and their C9 methyl groups are engaged in C9–H···O5 interactions, i.e., C91–H···O55 and C95–H···O51 with C···O distances in the range 3.167–3.561 Å, Table A.7 (page 118), Figures 3.8(a)–(d) and 3.9(a). In addition, this water site is in close C–H···O type contact to both or only one C9 methyl groups of glucose units 2 and 6 in TRIMEG 2, 3, 4. In TRIMEG 1, however, such interactions are not found due to the large number of water positions which appear to impede these contacts. Furthermore, a number of C–H···O hydrogen bonds contribute to crystal structure stabilization as frequently observed in other carbohydrate structures [156] (see Table A.7 on page 118).

• **The Three Disconnected Water Clusters.** The 19.3 water molecules in the asymmetric unit are distributed over 27 sites. These sites are hydrogen bonded to form three clusters which are separated from each other (see Figures 3.8(a)–(d) and 3.10(a)–(c)). One of the clusters containing 10 water sites is bonded to TRIMEG 1 and 4, one cluster of 9 sites binds to TRIMEG 1 and 2, and the smallest cluster with 6 sites is bonded to TRIMEG 2 and 3. One individual water site, W3, binds to TRIMEG 1, and one, W16, to TRIMEG 2. The water sites are all in hydrogen bonding distance except for some water sites with low occupancies for which O···O distances are in the range 2.027–2.436 Å, i.e., these water sites cannot be occupied simultaneously, Figures 3.10(a)–(c). These short distances are W8···W10 and W9···W10 in Figure 3.10(a), W12···W13 and W13···W14 in Figure 3.10(b), and W21···W22, W21···W23, W25···W26 in Figure 3.10(c).

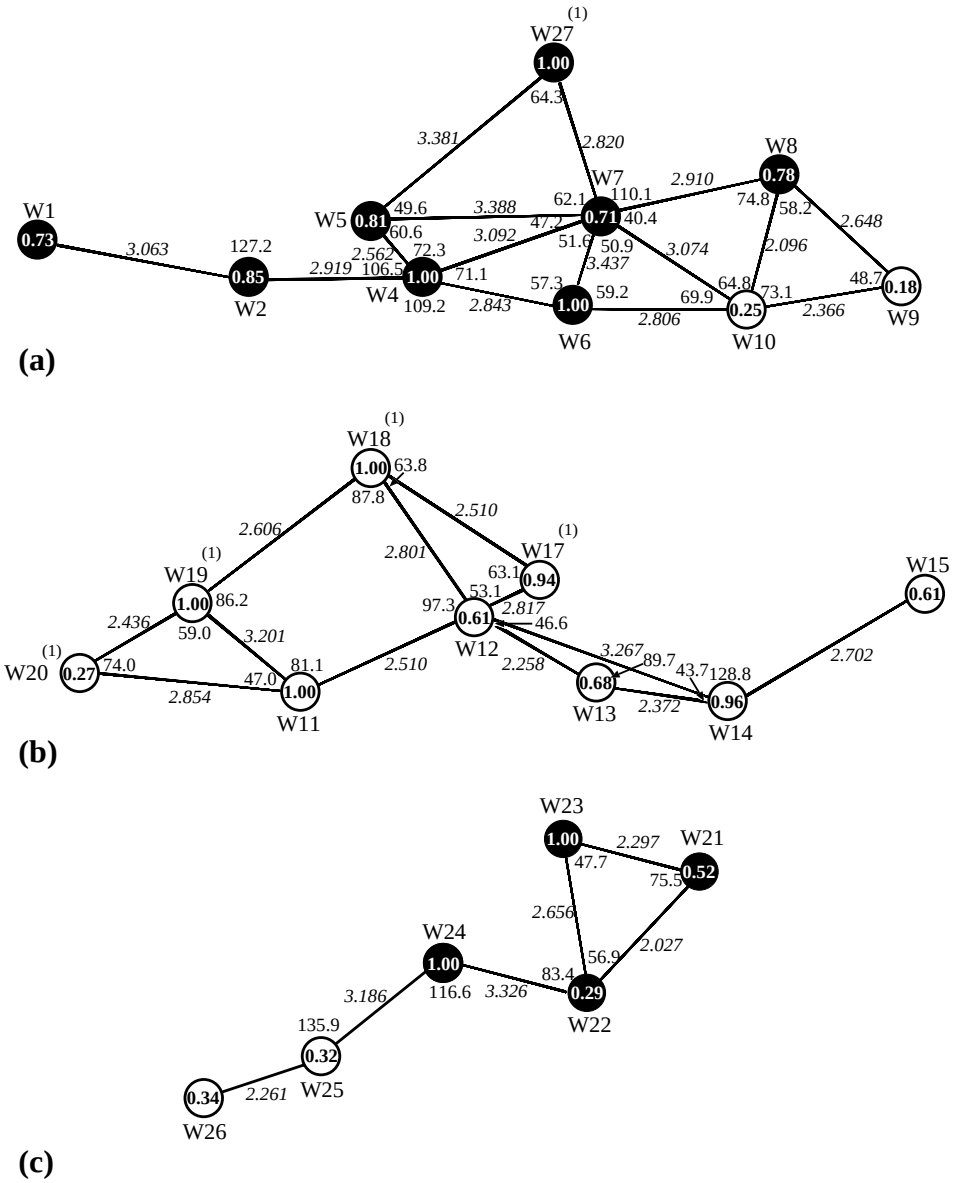

Figure 3.10: Three distinct water clusters in (4TRIMEG)·19.3H_2O (a) 10 water sites bind to TRIMEG 1 and 4, (b) 9 water sites bind to TRIMEG 1 and 2, and (c) 6 water sites bind to TRIMEG 2 and 3 (see also Figures 3.8(a)–(d)). The filled and unfilled circles describe the water sites which are inside and outside the TRIMEG cavities, respectively. The numbers written in the circles indicate the occupancy factors of water sites. Water sites with superscripts (1) indicate the symmetry equivalent position: $-1 + x$, y, z. Given distances in Å and angles in °.

• **TRIMEG Molecules are Differently Hydrated, with Some Common Patterns.** In all four TRIMEG structures, one water molecule is located on the pseudo-twofold axis as an integral part of their structures (TRIMEG 1, W2; TRIMEG

2, W16; TRIMEG 3, W23; TRIMEG 4, W27). The TRIMEG molecules are further hydrated, with some recurrent patterns (Figures 3.8(a)–(d):

(i) in TRIMEG 3 and 4, W24 and W8, respectively form hydrogen bonds to glucose units 5 and 6, involving O35, O56, O66;

(ii) one water site bridges O26 and O45 in TRIMEG 1, 2, and 3 (water W14, W19, and W26);

(iii) one water site bridges O6 of adjacent *syn*-oriented glucoses in TRIMEG 1 and 2: W6 bridges O62 and O63 in TRIMEG 1; W26 bridges O63A and O64B in TRIMEG 2; and

iv) two water molecules bridge O4 of *anti*-oriented glucose units 4 and 5 in TRIMEG 1 and 2: O44···W13···W14···O45 and O44···W18···W19···O45.

Summarized Structural Description of (4TRIMEG)·19.3H_2O. The four independent TRIMEG molecules have a similar elliptical shape with pseudo-twofold rotational symmetry. This conformation appears to be imposed and stabilized by the $\approx 180°$ flipping (*anti*-orientation) of the two diametrically opposed glucose units 1 and 5 whose C5–C6–O6–C9 chains are rotated towards the molecular cavity and have nearly identical conformations. This permits O61 and O65 to form hydrogen bonds to a water molecule (O_w) located on the pseudo-twofold axis and, in addition, there are systematic C–H···O interactions of type C91–H···O55 and C95–H···O51. These interactions close the molecular cavity from one side so that the TRIMEG molecules have a bowl-shaped form similar to other methylated CDs crystallized from hot water [25, 73, 155, 157, 158, 160], see Figures 1.15–1.19 (pages 26–28). The other side of the cavity is not closed but narrowed by "inward" rotation of O6–C9 groups of glucose units 2 and 6, a conformation stabilized by C9–H···O_w interactions to the water molecule O_w located on the pseudo-twofold axis. The hydration schemes of the four TRIMEG molecules differ from each other but some recurrent patterns are observed. Even O4 is engaged as a hydrogen bond acceptor, a feature which is rare in the native CDs. The reason is that the hydrogen bond accepting O4 are located on both sides (O44, O45) of the flipped glucose unit 5; thus, the O4 atoms become exposed and facilitate hydrogen bonding, as shown with TRIMEG 1 and 2.

3.1.2.1 TRIMEG·4.5H_2O

Molecular Structure of TRIMEG·4.5H_2O. The 8 glucose units of TRIMEG are all oriented *syn* and in the regular $^4C_1$ chair conformation as indicated by the Cremer-Pople parameters, Q and Θ [32], Table 3.4. The narrow variation of O4(n)···O4($n-1$) distances and the moderate deviation of the glycosidic O4 from their common least-squares plane indicate that the TRIMEG macrocycle adopts a "round" shape, but individual glucoses are tilted considerably as shown by their tilt angles (8.0–57.9°) and by the distribution of torsion angles around glycosidic O4, ϕ and ψ [2] in the ranges 76.8–126.1° and 87.2–157.1°, respectively (see Figure 3.11, and Table 3.4). This contrasts the known structures, TRIMEG·2H_2O [160] and (4TRIMEG)·19.3H_2O [13] where the macrocycles adopt "elliptical" shapes because diametrically opposed glucoses are flipped by ≈ 180° (*anti*), Figure 3.9. The systematic interglucose C6–H(n)···O5($n+1$) hydrogen bonds which usually contribute to the stability of the CD structures exist in only 6 contacts because for glucose residues 1 and 6 whose C6(n)···O5($n+1$) distances are too long and C6–H(n)···O5($n+1$) angles are too small to indicate such interactions (see Table 3.4).

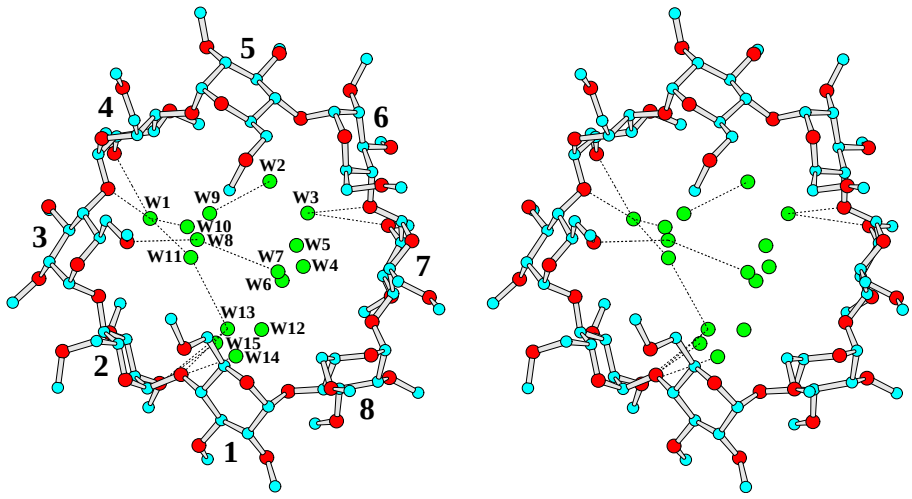

Figure 3.11: Stereo plot of TRIMEG·4.5H_2O
Carbon, oxygen, and water oxygen atoms as cyan, red, and green spheres, respectively; the seven glucose residues are labeled with numbers 1–8. Dotted lines indicate possible O–H···O hydrogen bonds within 3.5 Å distance. Water sites in the TRIMEG cavity are occupied as follows: W1, 0.50; W2, 0.40; W3, 0.60; all others 0.25.

Table 3.4: Geometrical parameters of the TRIMEG·4.5H_2O macrocycle
Distances in Å and angles in °. Definitions of puckering parameters: Q, Θ; torsion angles: ϕ, ψ; tilt angle; O4 angle, O4 deviation are explained in chapter 1 on pages 8–9.

Residue	1	2	3	4	5	6	7	8
Q	0.55	0.53	0.54	0.56	0.56	0.53	0.56	0.56
Θ	5	2	8	4	6	4	12	6
ϕ	113.2(12)	76.8(12)	115.2(10)	85.2(12)	126.1(11)	100.4(13)	94.0(11)	108.7(11)
ψ	152.7(10)	87.2(11)	155.2(10)	100.5(11)	157.1(10)	119.8(12)	107.9(12)	148.2(11)
Tilt angle	57.9(3)	8.0(8)	29.6(4)	10.9(4)	41.3(6)	22.7(8)	12.3(6)	28.1(5)
O4 angle	144.8(2)	128.5(2)	136.4(2)	134.1(2)	129.2(2)	140.9(2)	128.9(2)	126.0(2)
O4 deviation	0.01(1)	0.30(1)	0.29(1)	–0.43(1)	–0.37(1)	0.59(1)	0.33(1)	–0.73(1)
Distances								
O4(n)···O4(n – 1)	4.38(1)	4.52(1)	4.30(1)	4.57(1)	4.30(1)	4.54(1)	4.59(1)	4.39(1)
C6(n)···O5(n + 1)	3.97(2)[a]	3.23(1)	3.63(2)	3.50(2)	3.31(2)	3.90(1)[a]	3.15(2)	3.22(2)
H6(n)···O5(n + 1)	3.69(2)[a]	2.50(1)	2.85(2)	2.72(2)	2.48(2)	3.63(1)[a]	2.45(2)	2.42(2)
∠ C6–H(n)··· O5(n + 1)	99.5(8)[a]	132.5(8)	137.3(9)	138.1(8)	143.5(7)	98.5(8)[a]	129.0(8)	140.3(10)
Torsion angles								
C1–C2–O2–C7	95.0(13)	115.5(14)	71.3(14)	133.0(14)	113.5(14)	95.2(18)	127.9(15)	104.6(14)
C2–C3–O3–C8	–98.2(13)	–136.4(13)	–91.3(13)	–124.2(13)	–101.5(15)	–92.3(20)	–128.9(14)	–127.9(14)
O5–C5–C6–O6	–70.1(17)	–76.3(13)	74.4(15)	–70.2(12)	63.7(15)	–83.1(13)	–71.0(12)	–71.9(14)
C5–C6–O6–C9	175.6(15)	82.8(16)	–162.4(18)	174.1(11)	55.4(33)	157.4(19)	178.0(11)	126.3(21)

[a] C6(n)···O5(n + 1), H6(n)···O5(n + 1) distances too long and C6–H(n)···O5(n + 1) angles too small so that the systematic intramolecular, interglucose C6–H(n)···O5(n + 1) hydrogen bond probably not formed.

The orientations of methoxy groups, O2–CH_3, O3–CH_3, and O6–CH_3 are described by torsion angles in Table 3.4. All O2–CH_3, and O3–CH_3 methoxy groups point "away" from the TRIMEG cavity (Figure 3.11) as indicated by the torsion angles C1–C2–O2–C7 and C2–C3–O3–C8. The torsion angles O5–C5–C6–O6 of the glucose units 3 and 5 are +*gauche* whereas the others are –*gauche*, and all torsion angles C5–C6–O6–C9 are *trans* except for glucose units 2 and 5 which are +*gauche* (82.8° and 55.4°). Only O6–CH_3 of glucose residue 5 is directed "toward" the cavity so that the geometry of TRIMEG is not bowl-shaped but resembles more an open cylinder, see Figure 3.11. This agrees with previous structures of methylated CD crystals grown from cold water, DIMEA·H_2O [73] (Figure 1.20, page 29) and DIMEB·2H_2O [11, 12] (Figure 3.1, page 52). By contrast, in crystals obtained from hot water [25, 73, 155, 157, 158, 160] methylated CDs exhibit a bowl-shaped conformation because two or three O6–CH_3 groups are rotated "inward" and close the cavity from this side, see Figures 1.15–1.19 (pages 26–28).

The 4.5 Water Molecules are Included in the TRIMEG Cavity. A total of 4.5 water molecules are distributed over 15 positions of which none is fully occupied (occupancy factors 0.25–0.60), see Table A.4 on page 116. These water sites are located in the cavity of TRIMEG, Figure 3.11, none is found in interstices between TRIMEG molecules (Figure 3.12). The water sites are not evenly distributed in the TRIMEG cavity but form three distinct clusters consisting of four sites each: W4–W7; W8–W11; W12–W15. In these clusters, the distances between water sites, 1.23–1.77 Å, are so short that they cannot be occupied simultaneously and the occupancy factors are so low (0.25) that they add up to one water molecule for each cluster. The other distances between water sites indicated by dotted lines in Figure 3.11 are in the range 2.54–3.43 Å. Three of the water sites are hydrogen bonded to O4 and O2 of adjacent glucoses (2.92–3.50 Å), *viz* W1···O43/O24, W3···O46/O27 and W13···O41/O22. Hydrogen bonds to glycosidic O4 atoms are rare in CDs and formed here probably because O–CH_3 groups are weaker hydrogen bond acceptors than O4. The inclusion of water molecules in the TRIMEG cavity appears to stabilize the "round" structure, but glucose residues 1 and 5 are more tilted than the others (57.9° and 41.3°, Table 3.4), suggesting that they could easily flip into the *anti* conformations found in the other two TRIMEG structures [13, 160].

Crystal Packing. TRIMEG molecules are stacked head-to-tail and inclined about 70° against the *a*-axis. The central cavities form an infinite channel filled by water molecules, Figure 3.12. This molecular arrangement is similar to the pattern typical for native CDs in complex with long molecular or ionic guests where the channels are stabilized by intermolecular hydrogen bonds between O2–H/O3–H and O6–H [136]. For the present crystal structure however, such interactions cannot occur and the crystal lattice is stabilized by van der Waals contacts and C–H···O hydrogen bonds, the shortest being 3.50 Å between C93 (x, y, z) and O23 ($x + 1$, y, z).

TRIMEG·4.5H_2O is an Evidence for Conformational Flexibility of Permethylated CDs. The present structure shows that TRIMEG does not exclusively occur in the "elliptical" form found in TRIMEG·2H_2O [160] and (4TRIMEG)·19.3 H_2O [13], but it can also adopt the "round" form with all glucose residues oriented *syn*. This is the conformation found for native α-, β-, γ-CDs and for their methylated

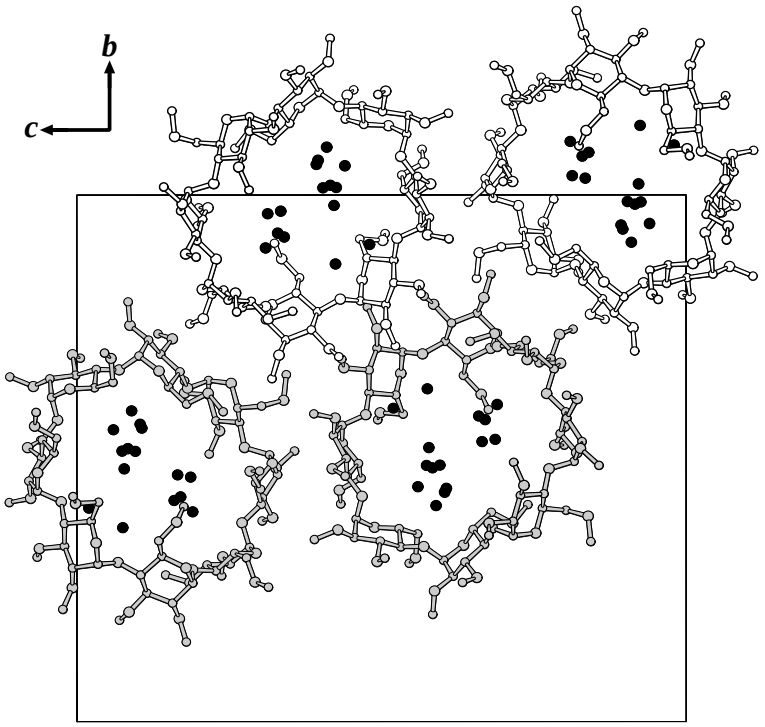

(a)

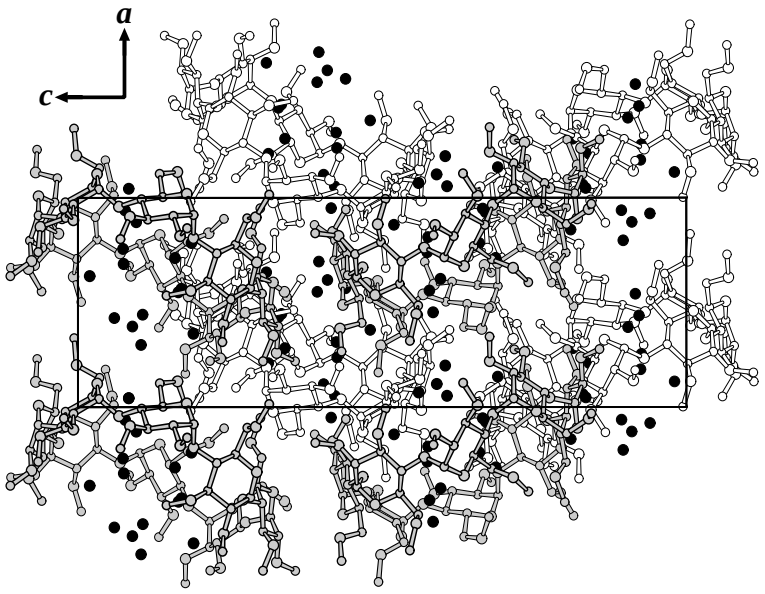

(b)

Figure 3.12: Packing in "head-to-head" channel style of TRIMEG·4.5H_2O (a) Top and (b) side views. TRIMEG molecules related by the twofold screw operation along the *b*-axis are shaded gray, filled circles are water molecules. Note that in Figure 3.12(b), TRIMEG molecules form an infinite channel parallel to the *a*-axis and that all water sites are located within the channels; none is between TRIMEG molecules.

derivatives and even for TRIMEB·H_2O [25], in which one of the glucose residues is "inverted" to a $^1C_4$ chair form. In both TRIMEG forms, the glucose residues are in a seemingly unstrained $^4C_1$ conformation (as indicated by the Cremer-Pople parameters) so that "elliptical" and "round" TRIMEG are energetically similar. This implies that in solution, both forms could coexist in equilibrium because the macrocycle is wide enough to permit rotation of individual glucose residues by $\approx 180°$ with only little or no steric constraints, contrasting the smaller native and methylated CDs in which all glucoses are oriented *syn*. Out of a variety of possible conformers of TRIMEG, the "elliptical" form appears to be energetically preferred, probably because it is stabilized by favorable intramolecular C–H$\cdots$O interactions involving glucose residues 1 and 5 in *anti* orientation (see dashed lines in Figure 3.9).

3.1.2.3 Structural Comparison of Uncomplexed TRIMEG

TRIMEG could be crystallized from aqueous solutions in three different forms, TRIMEG·4.5H_2O [7], (4TRIMEG)·19.3H_2O [13] at 18°C, and TRIMEG·2H_2O [160] at 80°C. The molecular conformations of TRIMEG in (4TRIMEG)·19.3H_2O and TRIMEG·2H_2O are similar in the "elliptical" bowl-like shapes with the cavities at O6-sides closed by "inward" rotation of O6–CH_3 groups of two flipped glucose units 1 and 5 at diametrically opposed positions, as indicated by the rms deviations of superpositions in the range 0.48–0.88 Å (see Figures 3.9(a)–(b)). In both, the O_w–H$\cdots$O6 hydrogen bonds play a crucial role in stabilizing the macrocyclic conformations, see Figure 1.19 (page 28) for TRIMEG·2H_2O and Figures 3.8(a)–(d) (page 66) for (4TRIMEG)·19.3H_2O.

The flipping of two glucoses into *anti* orientation is probably associated with the inability to form O2(n)$\cdots$O3($n-1$) hydrogen bonds which contribute to the stability of the *syn* orientation of glucoses if O2–H and/or O3–H hydroxyl groups are not methylated. For unmodified CDs, flipping of glucoses was only observed for the larger ϵ-CD [88, 89], ι-CD [88, 89], and ϕ-CD [59] with 10, 14, and 26 glucose units, respectively, where it served to reduce steric strain. In these larger CDs, however, the flip does not only involve one individual glucose as in TRIMEG. The appended glucoses are also flipped as they are all connected by O2(n)$\cdots$O3($n-1$) hydrogen bonds, and this is why this flip was termed "band flip" (like cutting a band, rotating one end by 180° and glueing the two ends together) [59, 88, 89].

In contrast to the "elliptical" bowl-like shapes of (4TRIMEG)·19.3H_2O and TRIMEG·2H_2O which are specifically stabilized by O_w–H···O6 hydrogen bonds, the TRIMEG·4.5H_2O adopts a "round" cyclinder-like form which is maintained by O_w–H···O hydrogen bonds of included water molecules. It is not obvious why this crystal form occurs and why it cannot be reproduced in crystallization experiments. However, the variety in conformations of TRIMEG suggests that this molecule is structurally flexibile (discussed above).

With respect to molecular hydration, the hydration numbers per TRIMEG are comparable in both forms crystallized from cold water: TRIMEG·4.8H_2O for (4TRIMEG)·19.3H_2O and TRIMEG·4.5H_2O. In both, water molecules are located mostly within or close to the TRIMEG cavities, while in TRIMEG·2H_2O crystallized from hot water the water molecules are located close to but not within the TRIMEG cavity.

3.1.3 Negative Solubility Coefficient in Water of Methylated CDs – A Paradigm of the Hydrophobic Effect

Albeit TRIMEG and DIMEB could be crystallized from cold water, their structural features and in particular the hydration patterns are different. This is because the fully methylated TRIMEG has lost the strong hydrogen bonding donor/acceptor functionality of the O3–H groups; they are replaced by the weak O3–CH_3 acceptors so that no intramolecular O3–H(n)···O2(n + 1) hydrogen bonds can form, rendering these molecules more flexible. This explains why in (4TRIMEG)·19.3H_2O [13] each of the four independent TRIMEG molecules shows an elliptical conformation with two diametrically opposed glucose units flipped from the common *syn* to *anti* orientation; their O6 atoms are now close enough to permit hydrogen bonding to a bridging water molecule. Additional water molecules are located inside and outside the cavities, hydrating the four TRIMEG individually: three to five $O_{TRIMEG}\cdots O_w$ hydrogen bonds connect TRIMEG to water clusters of different sizes and shapes. In an alternative form, TRIMEG·4.5H_2O [7], the molecule adopts a round conformation with all glucoses in *syn* orientation and stabilized by hydrogen bonding to the embedded water molecules. This differs from DIMEB·15H_2O [9] where the water molecules form a sophisticated, well organized hydrogen bonding network in a channel clathrate hydrate structure enclosing DIMEB. In addition, DIMEB·15H_2O [9] has no melting

point (m.p.) but exhibits extremely high thermal stability with decomposition at 280°C while (4TRIMEG)·19.3H_2O [13] has m.p. at *ca.* 124°C.

It is conceivable that the structures of DIMEB·15H_2O, (4TRIMEG)·19.3H_2O, and TRIMEG·4.5H_2O represent snapshots of hydrated DIMEB and TRIMEG in cold aqueous solutions, similar as found for trimethylamine decahydrate in crystalline and liquid states [46]. This would correspond to Pauling's clathrate hydrate model of liquid water [129], and to Jeffrey's "liquid analogy" to clathrate hydration [91]. Therefore, methylated CDs are well soluble in cold water probably because they are massively hydrated. At elavated temperatures, the hydration water molecules become more mobile and the macrocycles more flexible, leading to disruption of the hydration shells and crystallization of the hydrophobic, methylated CDs as DIMEB anhydrate [157] or TRIMEG·2H_2O [160].

The solubility behavior of methylated CDs can be attributed to the hydrophobic effect which is a controversial issue since 60 years [172]. Hydrophobic interaction plays an important role in stabilizing the macromolecular structures [172], especially proteins, as about three-quarters of the stabilizing free energy accounts for this interaction [143]. Therefore, understanding the water solubility of methylated CDs may further our understanding of the hydrophobic effect. Additional investigations on the aqueous solution of methylated CDs using the neutron scattering technique is described in the next section.

3.2 Neutron Scattering Study

3.2.1 Fitting of Pure Water Data

The fitting of theoretical to measured scattering functions of H_2O data at 287 and 305 K is satisfactory and the obtained dynamical parameters are reasonable as shown in Figure 3.13 and Table 3.5. For the data at 323 K which could not be used for analysing due to experimental problems, their dynamical parameters were obtained by extrapolation using the following equations:

$$(1/\tau_{trans})_T = 9884.23e^{-\frac{2693.874}{T}} \tag{3.1}$$

$$(D_{rot})_T = 1.187e^{-\frac{767.336}{T}} \tag{3.2}$$

$$(E_{DHO})_T = -0.04T + 19.656 \tag{3.3}$$

$$(\Gamma_{DHO})_T = -0.03T + 24.6 \tag{3.4}$$

Note that in principle, E_{DHO} and Γ_{DHO} should be temperature independent according to susceptibility measurements (by Longeville [116]) which are 8 and 12 meV, respectively. However, for the present data the best fit could not be obtained with these values, and therefore they were redetermined and found to be inversely proportional to the temperature (Table 3.5).

The parameters obtained in this study agree well with those of Teixeira *et al.* [173] at the temperatures 287 and 305 K (Table 3.5). At 323 K, greater discrepancies can be observed because Teixeira's values are obtained by extrapolation (out of the measured temperature range, 253–293 K) therefore, they may be incorrect. Furthermore, the present analytical model has been improved, e.g., the MSC correction is included, $\langle u^2 \rangle$ are treated as temperature dependent values which are more reasonable than the temperature independent value of Teixeira (Table 3.5). The inelastic scattering is taken into account by the DHO function parameters: $\langle u^2 \rangle$, energy, and damping which are neglected in Teixeira's treatment [173]. Therefore, it is probable that the water dynamical parameters determined in this study are more precise and reliable.

It is apparent that the temperature evolution of the water dynamics is well described. Obtaining the reliable parameters of the remaining contribution to the measured spectral intensity of CD solution ($< 10\%$ for CD and its hydration water, see fractions ($F_{CD} + F_{hyd}$) in Figure 2.1 on page 45 and Table 3.6 on page 85) is important for understanding the solubility in water of CD.

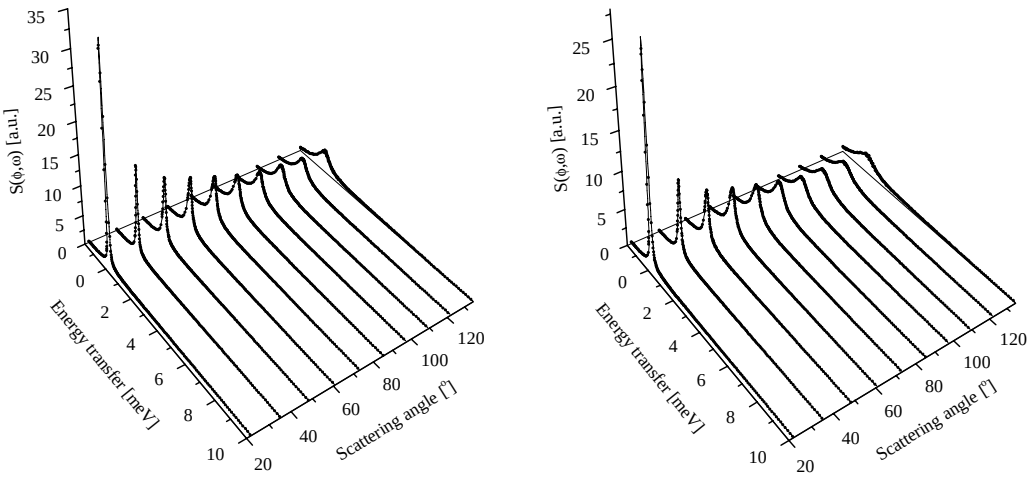

(a) 287 K (b) 305 K

Figure 3.13: Neutron scattering spectra of H_2O at 287, 305 K
Comparison between the theoretical scattering functions, $S_{theo}(\phi,\omega)$, line shapes (–) and the measured scattering functions, $S_{meas}(\phi,\omega)$, (•) as a function of the scattering angle, ϕ [°] and the energy transfer, E, $\hbar\omega$ [meV] for pure water at (a) 287 K and (b) 305 K.

Table 3.5: Dynamical parameters of H_2O at different temperatures
Values in parentheses taken from Teixeira *et al.* [173] – those of 305 and 323 K are extrapolated from the corresponding values determined in the temperature range 253–293 K. D_{trans} and τ_{trans} are coefficient and relaxation time of translational diffusion; L is jump distance ($= \sqrt{6 D_{trans}\tau_{trans}}$). D_{rot} is rotational diffusion coefficient, $\langle u^2\rangle$ is mean square displacement, E_{DHO}, and Γ_{DHO} are energy and damping of the DHO function. For more details of these expressions, see the experimental section of neutron scattering, page 42.

Parameter	τ_{trans} (ps)	$D_{trans}\times10^{-5}$ (cm^2 s^{-1})	L (Å)	D_{rot} (meV)	$\langle u^2\rangle$ Å^2	E_{DHO} (meV)	Γ_{DHO} (meV)
287 K	1.20(1.6)	1.67(1.73)	1.10(1.29)	0.082(0.087)	0.221(0.078)	8.17	16.0
305 K	0.69(0.9)	2.64(3.08)	1.05(1.29)	0.096(0.104)	0.235(0.078)	7.45	15.45
323 K	0.42(0.5)	3.87(5.55)	0.99(1.29)	0.110(0.125)	0.249(0.078)	6.73	14.9

3.2.2 Fitting of CD Solutions Data

The fitting quality of theoretical to measured scattering functions of CD solutions is high and comparable to that of pure water as can be seen from Figures 3.14(a)–(c) which show the overall fitting of the neutron scattering spectra at 323 K (see

Figures B.2, B.3, B.4 for at other temperatures on pages 123–125).

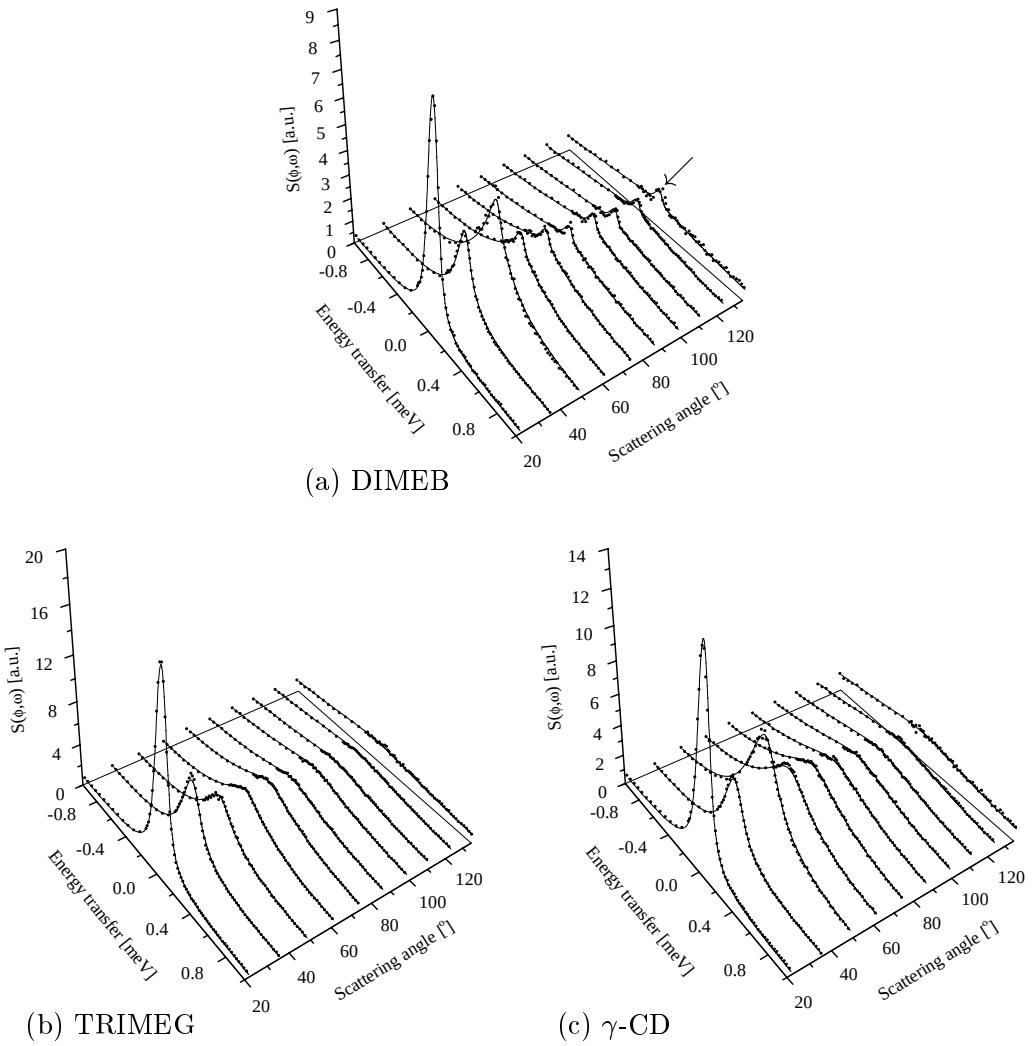

Figure 3.14: Neutron scattering spectra of CD solutions at 323 K
Comparison between the theoretical scattering functions, $S_{theo}(\phi, \omega)$, line shapes (–) and the measured scattering functions, $S_{meas}(\phi, \omega)$, (•) as a function of the scattering angle, ϕ [°] and the energy transfer, E, $\hbar\omega$ [meV] for aqueous solutions of (a) DIMEB, (b) TRIMEG, and (c) γ-CD. For clarity, only $-1 \leq E \leq 1$ meV is shown (see Figures B.2, B.3, B.4 for full E-range on pages 123–125). Arrow indicates the sharp elastic peaks due to scattering from DIMEB which is partially crystallized (5.5% of the original amount) at 323 K.

Note that the scattering intensity decreases with increasing scattering angle, ϕ (Figure 3.14) due to the attenuating effect of vibrations which is accounted by the DWF, $e^{-\langle u^2 \rangle Q^2}$ (eqn 2.6 on page 44) (the relation between Q and ϕ: $Q = 4\pi sin(\phi/2)/\lambda_0$).

In addition, regarding to the spectra with the same scattering angle, the scattering intensity decreases with increasing temperature (Figure 3.15), predicted by the factor $e^{-\frac{\hbar\omega}{2k_BT}}$ in eqn 2.5 (page 43).

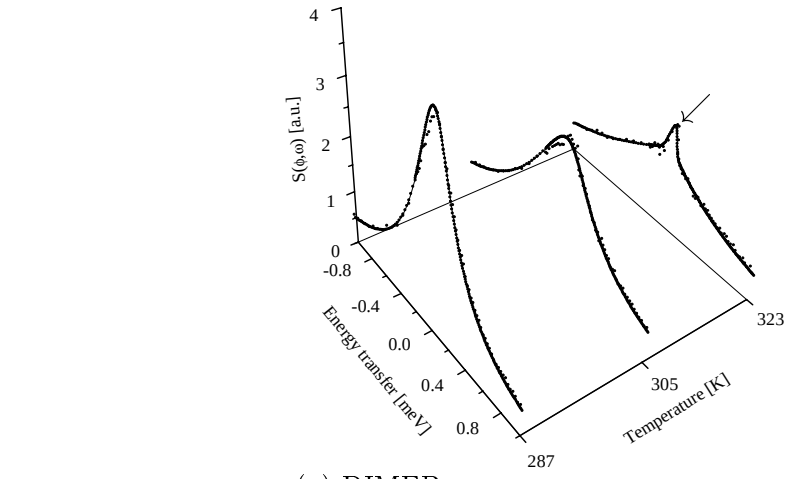

(a) DIMEB

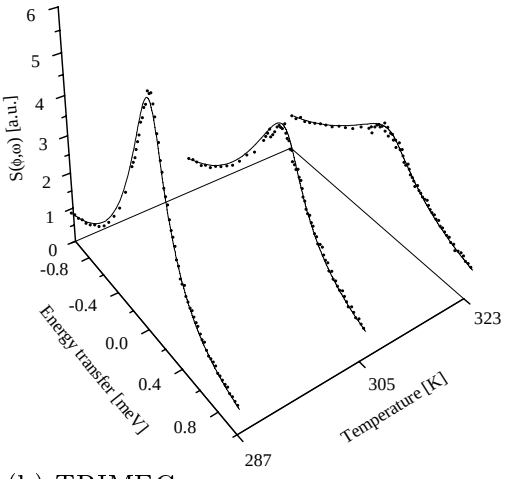

(b) TRIMEG

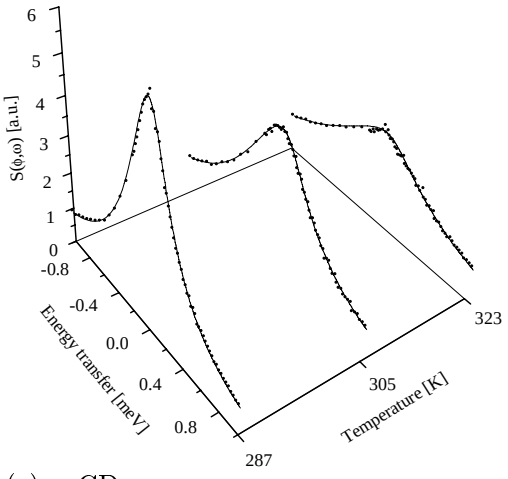

(c) γ-CD

Figure 3.15: Neutron scattering spectra of CD solutions at 287–323 K
Comparison between the theoretical scattering functions, $S_{theo}(\phi,\omega)$, line shapes (–) and the measured scattering functions, $S_{meas}(\phi,\omega)$, (•) as a function of the temperature at $\phi = 97.43°$ for the aqueous solutions of (a) DIMEB, (b) TRIMEG, and (c) γ-CD. For clarity, only $-1 \leq E \leq 1$ meV is shown (see Figures B.2, B.3, B.4 for full E-range on pages 123–125). Arrow indicates the sharp elastic peak due to scattering from DIMEB which is partially crystallized (5.5% of the original amount) at 323 K.

Figure 3.16 shows the deconvolution into different components of a spectrum of a CD solution. The total scattering function is an additive product of the four com-

ponents. The bulk water, hydration water, and CD exhibit diffusive motions so they contribute mostly in the quasielastic regime ($0 \leq E \leq 3$ meV) while the DHO function is accounted for the vibration in the inelastic regime ($E > 3$ meV). In addition, this figure is an example indicating the excellent agreement between the experimental data points and the theoretical scattering function based on the current model.

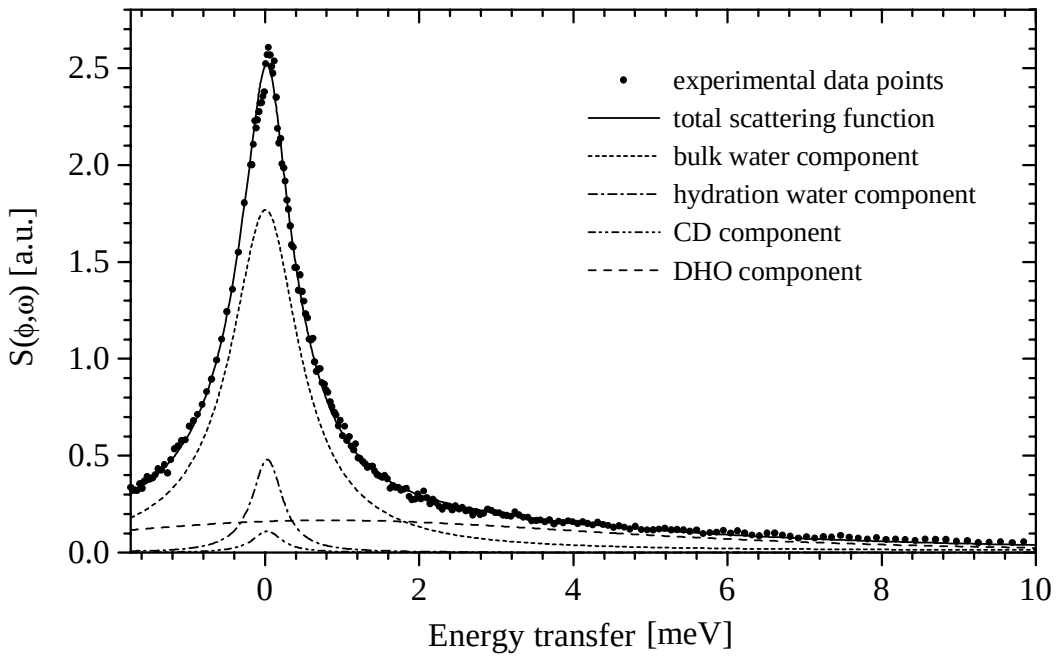

Figure 3.16: Composition of individual fitted CD solution spectra
The theoretical scattering function, $S_{theo}(\phi, \omega)$ (solid line) is a sum of scattering from translational and rotational diffusions of three components in quasielastic regime ($0 \leq E \leq 3$ meV), bulk water (short dashed line), hydration water (dashed-dotted line), CD (dashed-dotted-dotted line) and a component of DHO (long dashed line) in inelastic regime ($E > 3$ meV); the filled circles represent the measured scattering function, $S_{meas}(\phi, \omega)$. Shown is the spectrum of DIMEB solution at 305 K, $\phi = 97.43°$.

In the course of data analysis, a number of analytical models have been tested to verify whether it is possible to obtain a comparable fitting quality without contribution from hydration water. Indeed, the answer is *no!* It is clearly observed that when $F_{hyd} = 0$, the EISF intensity of the fitted spectra is missing if the other previously determined parameters are fixed. And even though they are allowed to reoptimize, the fitting quality is only slightly improved when compared to the former

test. This suggests that one needs to increase the rotation radius of the CD molecule in order to gain the EISF intensity back and obtain a better fit. To increase the CD rotation radius is an analogy to adding the hydration water as an integral part covering the CD macrocycle. Furthermore, to realize the model, the hydration water not only concerns the water molecules "outside" but also the ones embedded in the CD cavity. This is supported by crystallographic evidence that about six water molecules can be included in the CD cavity, suggesting that in the liquid state, the CD cavity is filled with water molecules. Therefore, the value of 0.004 for F_{hyd}^{in} is used as a starting point to be reoptimized in the fitting procedure. As shown in Table 3.6, the final values of F_{hyd}^{in} are slightly decreased from 0.004 (at 287 K) to 0.003 or 0.002 (at 323 K); this shows that the water molecules are confined in the CD cavity and are less dependent on the temperature when compared to the hydration water outside the cavity (F_{hyd}^{out}).

The characteristics of the jump diffusion model is demonstrated by the Q dependence of the quasielastic linewidth (HWHM) in Figure 3.17. By plotting HWHM^{-1} against Q^{-2} which is a linear function according to the equation: $\mathrm{HWHM} = D_{trans}Q^2/(1+D_{trans}Q^2\tau_{trans})$, the translational diffusion coefficient (D_{trans}) and relaxation time (τ_{trans}) can be determined (see the insets of Figure 3.17). It is obvious that the diffusion mobility of hydration water (and CD) is smaller than that of bulk water at all temperatures, see the summarized dynamical parameters in Table 3.6.

3.2.3 Dynamical Property of CD Solutions

At 287 K, the CDs show similar behavior in water as they are hydrated by a number of water molecules and diffuse with slightly different D_{trans} of 0.68, 0.65, and 0.77×10^{-5} $\mathrm{cm^2s^{-1}}$ for DIMEB, TRIMEG, and γ-CD – this corresponds to their number of H-atoms in the fractions which diffuse together ($F_{hyd}+F_{CD}$) of 0.066, 0.066, and 0.048, respectively, see Table 3.6 and Figure 3.18(a). Such diffusive motion is characteristic of the liquid state as indicated by the broad quasielastic peaks in Figure 3.15. The obtained hydration number (equal to $n_{hyd}/2$) of DIMEB is 52.1 molecules, much higher than those of TRIMEG and γ-CD (36.6 and 33.8 molecules, respectively), Table 3.6. This is consistent to their aqueous solubility at RT which are 57, 48, and 23 g/100 mL, respectively (Table 1.5 on page 21), and shows that DIMEB is more soluble than the others because it is heavier hydrated. Furthermore, the result from

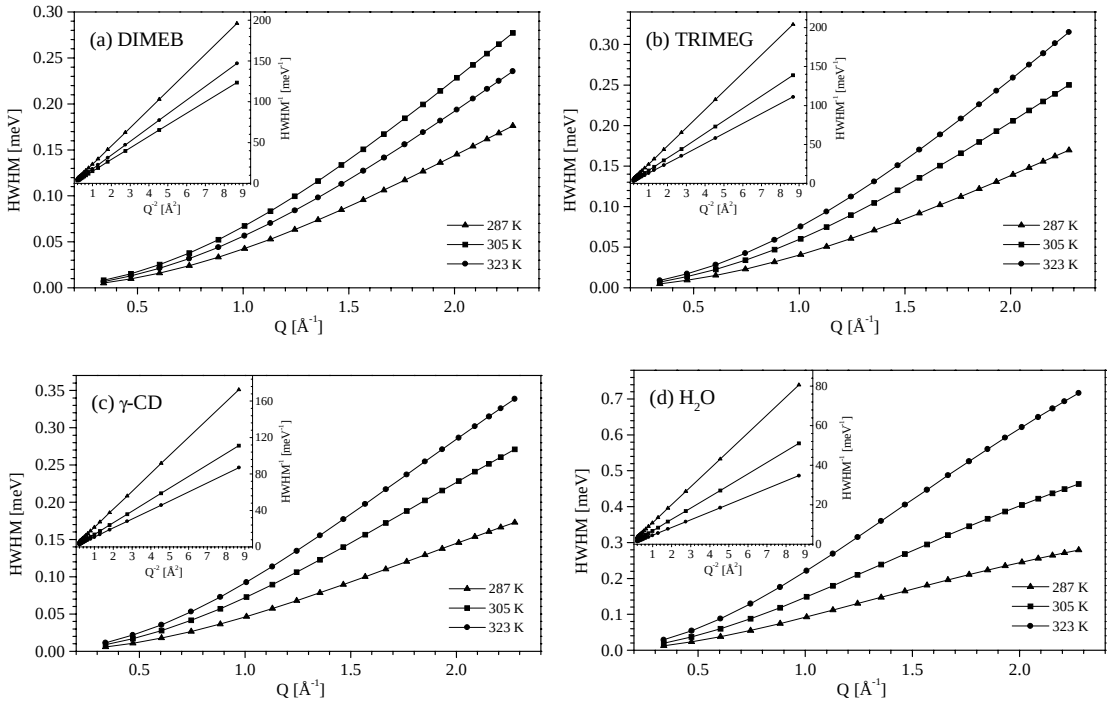

Figure 3.17: HWHMs of CD solutions and H_2O at 287–323 K
Half width at half maximum (HWHM) versus Q of (a) DIMEB, (b) TRIMEG, (c) γ-CD solutions, and (d) H_2O at: 287 K (triangle), 305 K (square), and 323 K (circle). Inset shows a plot of HWHM^{-1} versus Q^{-2}, of which the translational diffusion coefficient (D_{trans}) and relaxation time (τ_{trans}) are obtained from the reciprocal slope and y-intercept of the equation: $\mathrm{HWHM} = D_{trans}Q^2/(1 + D_{trans}Q^2\tau_{trans})$.

NMR has shown that in solution at RT, a glucose possesses the hydration number of 7.2 molecules [177]; this fairly agrees with the values obtained in this study (7.4, 4.6, 4.2 for DIMEB, TRIMEG, γ-CD; see the caption of Table 3.6).

When the temperature increases to 305 K, the hydration is perturbed and some water molecules which have weaker interaction to the CD macrocycle move from the hydration region to the bulk phase, consequently the hydration number is reduced and the fractions ($F_{hyd} + F_{CD}$) diffuse faster. DIMEB loses much more number of water in the hydration shell compared to the others (Table 3.6 and Figure 3.18(b)) because its solubility decreases considerably (> 60 g/100 mL (287 K) $\rightarrow \approx$ 40 g/100 mL (305 K), see Figure 1.13 on page 24). Albeit the solubility of TRIMEG decreases but γ-CD increases with increasing temperature however, no significant difference in dynamics between these two compounds can be observed at 305 K (as their hydration

Table 3.6: Dynamical parameters of CD solutions at different temperatures
CD and its hydration water diffuse together in a solution with the same dynamical parameters for both translation and rotation, see Table 2.3 for the rotation radii of CD and hydration water. Mean square displacements, $\langle u^2 \rangle$ are 0.225, 0.239, and 0.253 Å^2 at the temperatures 287, 305, and 323 K, respectively. DHO function parameters are the same as those of pure water at 287 and 305 K (Table 3.5), except at 323 K where the DHO energy and damping are 7.3, 13.28 meV for DIMEB; 7.3, 13.7 meV for TRIMEG; and 7.15, 12.5 meV for γ-CD. *Italic* and **bold** numbers are the fractions of hydration water inside and outside the CD cavity, F_{hyd}^{in} and F_{hyd}^{out}; they are summed up to F_{hyd}. Hydration number is equal to the number of H-atoms in hydration water fraction divided by two ($n_{hyd}/2$) and is temperature dependent: 52.1(7.4), 42.9(6.1), 16.8(2.4) for DIMEB; 36.6(4.6), 32.0(4.0), 27.4(3.4) for TRIMEG; 33.8(4.2), 29.3(3.7), 29.3(3.7) for γ-CD (listed in the temperature order of 287, 305, 323 K; values in parentheses are per one glucose unit). Fractions $F_x; x = hyd, CD$ are defined as $F_x = n_x/n_{tot}$ where n_{tot} is the total number of H-atoms in the representative unit of CD solution (Figure 2.1, page 45): 3053.4, 3083.4, and 3035.4 for DIMEB, TRIMEG, and γ-CD, respectively.

Sample	T (K)	τ_{trans} (ps)	$D_{trans} \times 10^{-5}$ (cm^2 s^{-1})	D_{rot} (meV)	Hydration water		CD		$F_{hyd} + F_{CD}$
					F_{hyd}	n_{hyd}	F_{CD}	n_{CD}	
DIMEB	287	0.90	0.68	0.002	0.034 *0.004* **0.030**	104.1	0.032	98	0.066
	305	0.57	1.07	0.004	0.028 *0.004* **0.024**	85.8			0.060
	323	0.65	0.90	0.003	0.011 *0.002* **0.009**	33.7			0.043
TRIMEG	287	0.91	0.65	0.001	0.024 *0.004* **0.020**	73.1	0.042	128	0.066
	305	0.62	0.96	0.003	0.021 *0.004* **0.017**	64.0			0.063
	323	0.48	1.20	0.005	0.018 *0.003* **0.015**	54.9			0.060
γ-CD	287	1.30	0.77	0.002	0.022 *0.004* **0.018**	67.7	0.026	80	0.048
	305	0.82	1.20	0.004	0.019 *0.003* **0.016**	58.5			0.045
	323	0.69	1.54	0.006	0.019 *0.003* **0.016**	58.5			0.045

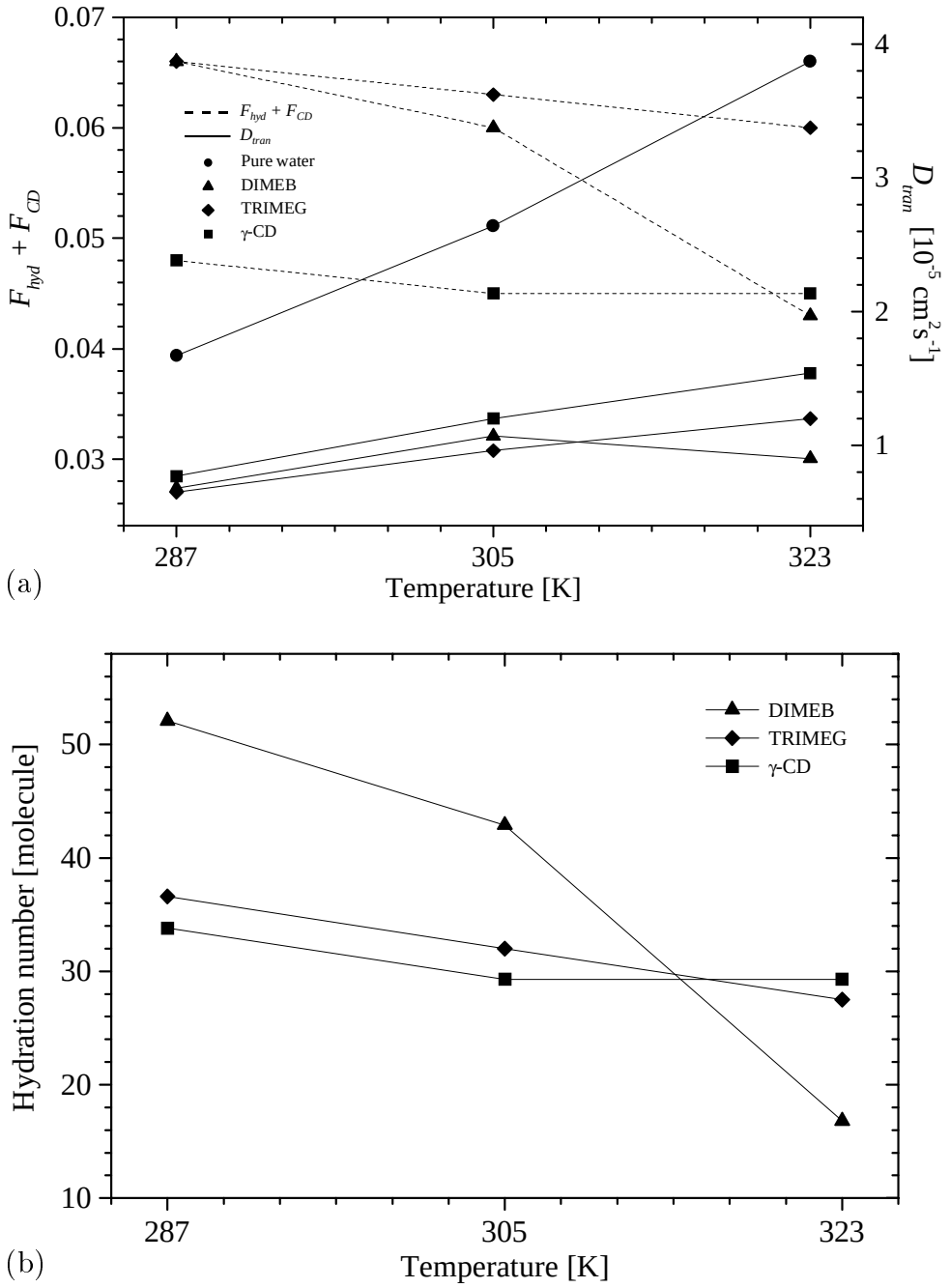

Figure 3.18: Values of (a) D_{trans}, $F_{hyd} + F_{CD}$ and (b) hydration number as a function of the temperature for each CD solution

In (a) the solid lines indicate the translational diffusion coefficient, D_{trans} (right axis) and the dashed lines show the sum of fractions of hydration water and CD, $F_{hyd} + F_{CD}$ (left axis). In (b) the fractions of hydration water both inside (F_{hyd}^{in}) and outside (F_{hyd}^{out}) the CD cavity are counted for the hydration number. Circle, triangle, diamond, and square denote the corresponding values of pure water, DIMEB, TRIMEG, and γ-CD solutions, respectively. Further detail see Table 3.6.

numbers and D_{trans} change in the same manner), Table 3.6, Figures 3.15 and 3.18.

At 323 K, DIMEB crystallizes partially (5.5% of the original amount according to the intensity of elastic peak) as indicated by a sharp elastic peak (see arrows in Figures 3.14(a) and 3.15(a)) which is a clear evidence for the very slow motion of large aggregates (probably crystalline) of DIMEB at this temperature. This agrees well with the observation that anhydrous DIMEB [157] crystallizes under these conditions. In the DIMEB solution (excluding crystalline DIMEB), the hydration number is continuously diminished (only 16.9 water molecules remain) and DIMEB diffuses slower, D_{trans} decreasing from 1.07×10^{-5} (305 K) to 0.90×10^{-5} cm^2 s^{-1} (323 K), Table 3.6 and Figure 3.18(a). This indicates that the DIMEB molecules form aggregates throughout the solution (the solubility at 323 K $\approx$ 14 g/100 mL, see Figure 1.13 on page 24). The dynamical behavior of DIMEB in aqueous solution has recently been demonstrated by molecular dynamics simulation that gives more detail toward the distribution of hydration water around the hydrophobic O–CH_3 and hydrophilic O–H groups of DIMEB [154]. At 298 K, DIMEB is hydrated by a large number of water molecules, more crowded around the hydrophobic groups compared to the hydrophilic groups. As the temperature increases to 343 K, the hydration number is substantially diminished, especially around the hydrophobic groups. The hydrophobic hydration shows the existence of a water "cage" structure (clathrate) around the apolar groups [150].

In contrast to DIMEB which crystallizes at 323 K, TRIMEG remains soluble because sufficient number of water molecules (27.4) hydrate the CD macrocycle, Table 3.6 and Figure 3.18. At higher temperatures (around 353 K) where TRIMEG crystallizes as dihydrate [160], similar dynamical behavior may be observed as in case of DIMEB. γ-CD which has normal solubility properties, i.e., positive solubility coefficient, is more soluble at 323 K and exhibits fastest diffusive motion among the three samples (Table 3.6 and Figure 3.18(a)). As the temperature rises, γ-CD remains soluble because there is a certain hydration number tightly bound to the CD macrocycle and is not stripped off even if the solution temperature is higher. The temperature evolution of the hydration number of γ-CD is: 33.9 (287 K) $\rightarrow$ 29.3 (305 K) $\rightarrow$ 29.3 (323 K), i.e., the hydration number reaches an asymptotic value of 29.3 water molecules at 323 K. Since γ-CD has three O–H groups per one glucose unit, hydrogen bonds are formed with the water molecules, yielding a threshold hydration number of

3.7 water molecules per one glucose unit, Table 3.6. This finding agrees with the results from a hydration dynamics study on poly(ethylene glycol) (PEG) using Raman spectroscopy [33] and ultrasonic velocity, and density measurements [90], showing that in PEG solutions, the hydration number decreases with increasing temperature at medium temperatures and converges to a definite value at higher temperature.

Although the present model gives a perfect fit of theoretical curves to the data and rational temperature evolution of D_{trans}, the value of D_{rot} is likely to be underestimated. In principle, D_{rot} of CD (and hydration water) should be $\approx$ 0.008–0.010 meV because the rotation radius of CD is about 10 times larger than that of bulk water (see Table 2.3 on page 50). However, the obtained D_{rot} in the range of 0.001–0.006 meV seems to be small; this indicates that other parameters, e.g., D_{trans}, F_{hyd} should be adjusted. As mentioned previously, there is a total number of 20 grouped, corrected spectra from the 388 recorded spectra in the scattering angle range 13.3–136.7°, therefore analysing these data is non-trivial. Furthermore, the assumption of decoupling between translational and rotational diffusions of water has limited validity at the measured temperature range (287–323 K) [173]. To obtain better agreement between the different parameters, small angle neutron scattering (SANS) experiment of the same CD solutions (but in D_2O) at different temperatures has been performed. The data analysis of SANS is in progress and in the very near future, the precise D_{trans} and D_{rot} of CD in the solution can be obtained so that the other parameters, especially F_{hyd} of the present data can be more reliably determined.